Laghi di Monticchio (Southern Italy, Region Basilicata): genesis of sediments—a geochemical study

Georg Schettler[1] and Patrick Albéric[2]

(1) GeoForschungsZentrum Potsdam, Section Climate Dynamics and Sediments, Telegrafenberg C328, 14473 Potsdam, Germany
(2) Institut des Sciences de la Terre d'Orléans (ISTO), UMR 6113 CNRS-Université d'Orléans, Bâtiment Géosciences, BP 6759, Rue de St Amand, 45067 Orléans Cedex 2, France

Abstract The sedimentation record of Lago Grande di Monticchio (LGM) is one of the most prominent paleoclimatic archives in the non-glaciated areas of Europe. However, the modern lake system has never been the subject of intense limnological studies. On the basis of hydrochemical water profiles, detailed investigations of sediment short cores and in situ pore water profiles from the littoral to the profundal zone, we elucidate spatial variations of sediment genesis within the lake basin and the importance of various depth sections for the lake's internal nutrient cycling. Sediments from the smaller meromictic Lago Piccolo di Montichio are discussed as a reference. Our study demonstrates: (i) distinctly higher sediment accumulation for the centre of the lake basin by focussing of the settling particle flux; (ii) decline of carbonate from the littoral to the profundal zones; (iii) non-synchronous change of calcite net-accumulation for various water depths; (iv) exceptionally high cation release from sediments covering the steeply inclining sector of the lake basin; (v) relatively constant dissolved silica concentrations in the pore waters (SiO_2 ~42 mg/l) independent of water depth and sediment composition; (vi) influx of oxygen-bearing groundwater into the anoxic hypolimnion after heavy rainfall and the associated precipitation of Fe-oxihydroxides; (vii) higher release of NH_4 by anaerobic degradation of organic matter at a water depth of 23 m than for sediments at a maximum water depth of 32 m, whereby the latter reflects the importance of seasonal sediment re-oxidation for anaerobic degradation of organic debris; (viii) although seasonal re-oxidation of sediments from various water depths is quite different, Oxygen Index values of LGM sediments fall in a small range, which reflects rapid microbial consumption of seasonally re-generated easily bio-degradable organic molecules.

Keywords Lacustrine sediments - Geochemistry - Genesis

Introduction

Sediment from Lago Grande di Monticchio (LGM, Fig. 1a–c) represents one of the most prominent European terrestrial paleoenvironmental archives with a continuous 100 kyr record spanning the Eem interglacial to the modern industrial period (Allen et al. *1999*). During the last decade, a reliable chronology for the LGM sedimentation record has been developed based on varve counting, AMS ^{14}C-dating, and tephrochronostratigraphy (Newton and Dugmore *1993*; Zolitschka and Negendank *1993*, *1996*; Narcisi *1996*; Huntley et al. *1999*; Wulf et al. *2004*). Contributions to local vegetation development as a mirror of paleoclimate change have been given by Watts (*1985*), Watts et al. (*1996a*, *b*, *2000*), Huntley et al. (*1999*) and Allen et al. (*2000*, *2002*). Diatom assemblages in LGM sediments as a proxy for paleoenvironmental change were investigated by Nimmergut et al. (*1999*). A pioneering geochemical study of a 50 m sedimentation record from LGM was done by Robinson (*1994*). Further geochemical sediment profiles were published by Creer and Morris (*1996*), Ramrath

et al. (*1999*) and Brauer et al. (*2000*). Still missing is a deeper understanding of sediment genesis in LGM, which constrains paleoclimatic interpretation of geochemical and geomagnetic sediment profiles that are partially based on sediment cores from various water depths (see contributions by Creer and Morris *1996*; Brandt et al. *1999*).

Here, a study of the modern LGM, based on snapshots of thermal and chemical lake stratification, in situ pore water profiles and investigation of short sediment cores taken along a transect from the littoral zone to the centre of the lake during summer stratification, is presented. The study was carried out to assess: (1) principal differences in sediment characteristics at various water depths, (2) differences in sediment accumulation between the shallow water area and the centre of the lake basin, (3) geochemical implications for groundwater inflow, (4) post-depositional redistribution of chemical elements and (5) the importance of various depth sections for the nutrient and sulphur cycle in LGM.

Geological setting and hydrological conditions

The Laghi Grande and Piccolo di Monticchio are maar lakes embedded in a collapsed structure on the southwestern slopes of the Monte Vulture volcanic complex (Fig. 1c). The suite of the local volcanic rocks is divided into two major units: the older Monte Vulture complex and the younger Monticchio unit. The oldest volcanic products of the Monte Vulture are the Foggianello sub-unit deposits of Fara d'Olivo ignimbrite (Crisci et al. *1983*). The Fara d'Olivo trachytic ignimbrite exhibits an age of 742 ± 11 kyr after Villa (*1988*). Buettner et al. (*2006*) suggested an age of 740 ± 7 kyr for the lower and <740 kyr for the upper Fara d'Olivo unit. The largest local volcanic rocks by volume are primary and epiclastic deposits of the Barile unit. Volcanic products of this unit were ejected between ca. 673 and 610 kyr BP (see Table 7-2 in Buettner et al. *2006* and references therein).

After a period of quiescence, the Monte Vulture volcano became dismembered by faulting (Valle dei Greggi-Fosso del Corbo fault system). Volcanism resumed with volumetrically subordinate eruptions assigned to the Monticchio unit (Laghi di Monticchio unit: 132 ± 12 kyr, Brocchini et al. *1994*; 141 ± 11 kyr suggested by Buettner et al. *2006*). Faulting caused subsidence of the southern half of the Vulture complex and collapse of its southwestern part. Eruptive activity of the Monticchio unit scattered along the active fault systems and was dominantly linked to diametric structures, two of which are located under the Monticchio Lakes (Giannandrea et al. *2006*).

The igneous rocks of the Vulture complex comprise phonolites, tephri-phonolites, phonolitic-foidites, and foidites (Principe et al. *2006* and references therein). Enhanced sulphur contents associated with the occurrence of hauyne $(Na,Ca)_{4–8}[Al_6Si_6O_{24}](SO_4,S)_{1–2}$ are peculiarities of these rocks. High SO_4 contents of Vulture lavas are thought to be caused by magma interaction with sedimentary SO_4-rich brines from the basement of the volcano covering Cretaceous to Pliocene sediments (La Volpe et al. *1984*; De Fino et al. *1986*). Substantial hydrothermal calcite, gypsum, and anhydrite vein deposits were detected during explorations in the hydrothermal fields of Tuscany and Latinum; Triassic marine evaporites are seen as the major SO_4 source of these mineralizations (Marini and Chiodini *1994* and references therein) and may also represent a major SO_4 source for hauyne-rich Vulture volcanites (see Table 1 in De Fino et al. *1986* for hauyne contents). This interpretation is supported by relatively positive $\delta^{34}S$ values of metasomatic hauyne phenocrysts (+6.1, +6.6‰) from the Vulture volcano (Cavarretta and Lombardi *1990*). According to an alternative explanation, the sulphate is primarily of magmatic origin: reduced sulphur became oxidized in the magma with

a high oxygen fugacity to SO_2/SO_3, and the escape of gaseous SO_2/SO_3 left heavy ^{34}S behind (see for detailed discussion Cavarretta and Lombardi *1990*). The Laghi di Monticchio unit, which is exposed in the western surroundings of LGM, involves a carbonatite-melilitite tuff sequence abundant in mantle xenoliths (Stoppa and Principe *1998*; Jones et al. *2000*; Downes et al. *2002*). Formation of the maar lakes is associated with phreatomagmatic eruptions during the final stage of volcanic activity.

The modern Lago Piccolo di Monticchio (LPM) has a maximum water depth of 38 m, a surface area of 1.6×10^5 m^2, and a water volume of 3.9×10^6 m^3 and receives sub-surface inflow from a catchment area of 1.05×10^6 m^2 (Zolitschka and Negendank *1996*). Lago Piccolo di Monticchio is meromictic with a chemocline at about 13 m (Chiodini et al. *1997* and references therein). Monimolimnion waters in LPM are anoxic with high CO_2 content and show a temperature increase with depth. Salinity increases to 1.8 g/l in the deepest part of the lake basin (monitoring data 1995: Chiodini et al. *1997*). The lake level of LPM is held artificially 1 m above the lake level of LGM (~656 m asl).

The surface area of the dimictic LGM is 4.05×10^5 m^2, and its water volume is 3.5×10^6 m^3 (Zolitschka and Negendank *1996*). The lake receives sub-surface drainage from a catchment of 3.04×10^6 m^2, including that of LPM, and has one outlet. The morphology of the LGM basin has been characterized by sonar measurements (Hansen *1993*). Lago Grande di Monticchio has an extended shallow area (Fig. 1b) with abundant submerged vegetation (*Ceratophyllum demersum*) and a littoral fringe rich in *Nympha alba* and *Polygonum amphibum*.

Mean annual precipitation (815 mm) is relatively high due to the elevation of the site (e.g. Monte Vulture: 1,262 m asl), although a pronounced dry period commonly occurs in the summer. The hillside is densely forested and dominated by Beech (*Fagus sylvatica*) and Turkey Oak (*Quercus cerris*) (Watts et al. *1996b*). A high percentage of precipitation does not drain but undergoes evapotranspiration. For an assumed evapotranspiration of 80% in the catchment, the above hydrological data suggest a water residence time of ~7 years for LGM. Loosely deposited pyroclastics in the catchment of LGM favour the seepage of precipitation. Drainage by surface runoff into the lakes, however, may occur during the melting of snow when the top-soils are frozen.

The lake level of LGM shows seasonal fluctuations, with high levels in early spring (pers. comm., local residents 1994). During late spring and summer, the lake level commonly decreases by one to two metres. Water level increase is limited by a canal built by monks of the monastery San Ippolito that was founded within the Piano Comune tuff ring depression in AD 1059 and discharges Lago Grande waters into the river Ofanto. During the winter of 1993/1994, both lakes were ice-covered. A clearly visible terrace, ca. 5 m above the modern lake level, indicates that the lake level was higher in the past. The lands surrounding Monte Vulture are cultivated, especially for cereals.

Sampling

On 22 August 1994 and 19 September 1994, temperature profiles of the water column were taken at the deepest part of both lakes. Divers placed dialysis cells along a transect (Fig. 1b) in the surface sediments of LGM at various water depths such that the uppermost dialysis chamber fit with the sediment/water interface (see Schwedhelm et al. *1988* for cell construction). The vertical distance between each chamber was 1 cm with 2 chambers at each

depth level. At each cell site, water samples were taken approximately 0.5 m above the surface sediment. To determine the amount of cations, an aliquot of the water sample was membrane-filtered (0.45 µm) and stabilized with nitric acid. Upon removal by divers on 19 September 1994, the single dialysis chambers were immediately sampled with syringes in 7 ml polypropylene tubes with a screw closure, manufactured by Sarstedt (Germany). One sample from each depth was stabilized by addition of 20 µl HNO_3.

Short gravity cores (□70 cm) were taken from the centre of lake LPM and along a transect (Fig. 1b) from LGM using a Niemistö gravity corer (Niemistö *1974*). The cores were continuously sampled at 3 cm slices by vertical extrusion; sample slices were immediately stored in a refrigerated box. Sediments from the deepest part of LGM had very high gas contents (methane), precluding taking a core from the deepest part of LGM.

Analytical methods

Water samples

The determination of fluoride, chloride, nitrate and sulphate was carried out by ion exchange chromatography (DX 100, Dionex). Soluble Reactive Phosphorus (SRP) and ammonium were determined colorimetrically (FIAS, Perkin Elmer) using the molybdenum-blue method for SRP measurements and spectro-photometry of an indicator solution after separation of NH_3 through a Teflon membrane (for details see Müller et al. *1992*). Dissolved inorganic carbon (DIC) of lake water samples was measured coulometrically. The DIC of pore water samples was determined by a commercial laboratory (ANTEUM, Berlin) by adding a small sample volume to phosphoric acid and performing IR-spectrometry of the released carbon dioxide (TOC 5000, Shimadzu). Dissolved silica and cations were measured sequentially by ICP-AES (ARL 35000). Temperature profiles of the lakes were taken by means of a water-tight single channel logger with an integrated thermistor temperature sensor (XL-100) manufactured by Richard Brancker Research, Canada.

Sediment samples

Sediment samples were frozen on return to the laboratory (1–2 days after sampling) and later freeze-dried. The <185 µm fraction was separated from the freeze-dried material by sieving. It comprised almost 100% of the total sample. After a $HNO_3/HClO_4$/HF/HCl-decomposition of 0.25 g solid sample, the determination of major and minor elements, including phosphorus and sulphur, was carried out by sequential ICP-AES (ARL 35000) and external calibration. Selected trace elements were measured by ICP-MS using a VG Plasma Quad PQ2+. Beryllium-9, ^{115}In and ^{187}Re were used for internal standardization. The total analytical errors for ICP-MS measurements were below ±10%. Inorganic carbon was measured coulometrically after decomposition with hot phosphorus acid (Coulomat 702, Ströhlein). The total carbon and nitrogen were determined after thermal decomposition at 1,350°C in an oxygen-gas-flow by IR-spectrometry and heat-conductivity detection, respectively (CNS 2000, LECO). Organic carbon was calculated by difference using the total and inorganic carbon results. Elemental sulphur was determined after methanol-extraction (reflux, 7 min) by reversed phase liquid chromatography (eluent: 80% methanol, column: C-18, UV-detection 254 nm, DX 100, Dionex, see Möckel *1984*). The chromatographic method enables the detection of polysulphides and sulphur of various chain- and ring-size, respectively. Octagonal ring-sized sulphur (S_8) was the dominant sulphur modification in the examined methanol-extracts. Only its peak area was considered for quantitative analyses of total elemental sulphur.

Rock-Eval (RE) pyrolysis was performed by means of a Turbo model RE6 pyrolyser (Vinci Technologies). Between 20 and 40 mg of freeze-dried sediments were analyzed using the "Recent Sediment" method in which the pyrolysis temperature (N_2 carrier gas) was increased from 200°C to 650°C at 30°C per minute. Basic RE parameters [Total Organic Carbon (TOC), Hydrogen Index (HI) and Oxygen Index (OI)] were calculated according to Espitalié et al. (*1985*) and Lafargue et al. (*1998*).

The mineralogical compositions of selected silt samples were determined by XRD-analysis of powdered samples (□1–5 μm) (Stoe Stadi-P diffractometer, Cu $K\alpha_1$ radiation). The Rietveld program GSAS was used for quantitative analysis (Larson and Von Dreele *1987*). Carbonates were dissolved with hot HCl (10%), organic matter was destroyed using H_2O_2 (30%) and >2 μm particles were separated by centrifugation prior analysis.

Radionuclides $^{210}Pb_{total}$, ^{137}Cs (661.66 keV) and the short-lived granddaughter nuclide ^{214}Pb (295.14 keV, 351.92 keV) of ^{226}Ra were measured using a high purity well-type germanium detector (model GCW3522, Canberra) at the given energies. Radiometric measurements were carried out at a lower sampling rate with less precision regarding counting statistics; γ-decays were typically counted for 1 g weight aliquots in sealed polypropylene tubes (45×15, Sarstedt, Germany) for 24 h, which corresponds to about 1,000 counts for ^{137}Cs at 100 mBq activity, and 800 counts for ^{210}Pb at 250 mBq. Lead-214 was typically measured at count rates between 200 and 800. Detector efficiency calibration for 46.539 keV was based on α-spectrometric measurements using a ^{208}Po recovery spike. Efficiency calibration for 295.14 keV and 351.92 keV was based on a gas-tight sealed Lab-internal powder standard that was spiked with ^{226}Ra (Amersham, RAXY.24). A mixture of radio-caesium spiked milk powder (Amersham, EUR-050) with an old sediment sample was used for efficiency calibration at 661.66 keV.

Results and discussion

Lake water characteristics

In the summer of 1994, LGM was characterized by high turbidity (Secchi-depth <30 cm) and elevated pH in the surface water (pH = 8.35, 18 September 1994, 18:30), whereas the epilimnion of LPM had clear water with high Secchi-depths (pH = 7.86, 19 September 1994, 10:00). The elevated pH in the surface water of LGM relative to LPM reflects higher uptake rates of dissolved CO_2 by primary producers. At the end of August 1994, a 5 m deep epilimnion (26°C) had developed in LPM, whereas a distinct warming (28°C) was only obtained in the upper 1–2 m of LGM due to the high turbidity in this lake (Fig. 2a, b). Below 1.5 m, temperature decreased to 6°C at a water depth of 14 m and was constant down to the lake bottom. The temperature of LPM was 7°C at a water depth of 13 m, increasing down to the lake bottom (10°C). The thermal stratification implies meromixis with an increase of salinity in the deep water. Meromixis of LPM could be confirmed by detailed hydrochemical investigations in the following year (Chiodini et al. *1997*). In both lakes, epilimnion temperatures decreased to 21°C until the middle of September 1994.

The epilimnion of LGM shows a distinct decline of Ca due to direct Ca uptake for calcification by biogenic uptake and biogenically induced calcite precipitation. The Mg profile of LGM shows a uniform pattern in August. There is no indication of significant co-precipitation of Mg with autochthonous calcite (Fig. 2c, d). Autochthonous calcite is characterized by high Ca/Sr. Consequently, Ca/Sr is lowered in the epilimnion of LGM and

the surface water of LPM is characterized by higher Ca/Sr than that of LGM (Fig. 2e). Equal DIC (total dissolved inorganic carbon) surface water concentrations in both lakes (~35 mg/l, Fig. 2f) imply that relatively higher deposition of autochthonous carbonate in LGM must be counter-balanced by the lake's internal carbon cycle and uptake of atmospheric CO_2. Increase of Ca and DIC in the hypolimnion of LGM towards the lake bottom reflects post-depositional dissolution of autochthonous carbonate. A pH decrease in the hypolimnion favours the chemical dissolution of settling $CaCO_3$ particles (see Fig. 2g, h for the increasing cation deficit in the ion budget if DIC is considered as HCO_3). LGM and LPM show unusually high Sr concentrations and low Ca/Sr and Na/Sr ratios (Sr: 0.6 mg/l, Ca/Sr: 75, Na/Sr: 60, Fig. 2e, i). Springs with such hydrochemical signatures are not typical for the entire Monte Vulture region (Barbieri and Morotti *2003*). Groundwater with these signatures is specifically obtained in springs near the Laghi di Monticchio (Fig. 1c). The above lake water characteristics may reflect dissolution of carbonates in the local carbonatite-melilitite tuff deposits, which show relatively low Ca/Sr ratios (Ca/Sr mass ratios: 36–298, Jones et al. *2000*). Dissolution of strontianite and coelistine in evaporatites from the sedimentary basement may further provide a major contribution to the high Sr contents of the local groundwater.

In LGM, Soluble Reactive Phosphorus (SRP) was not detectable down to a water depth of 6 m in August and down to 8 m in September (Fig. 3a). Primary production in both maar lakes is obviously limited by SRP availability. From August to September, SRP increased in the deep water of LGM by continuing SRP reflux from the surface sediments and PO_4 release from settling particles. Dissolved silica was depleted in the upper part of the water column by biogenic uptake to ca. 5 mg/l SiO_2, which was not limiting for the diatom growth (Fig. 3b). The surface water concentration of silica in LPM (30 mg/l SiO_2) distinctly exceeded that of LGM and was even higher than that of the deep water in LGM (20 mg/l). Lago Piccolo di Monticchio discharges into LGM, and a portion of the nutrient-rich groundwater discharge from the catchment reaches LGM via LPM, which acts as a sink for dissolved nutrients by biogenic uptake. Presuming that LGM and LPM are fed by groundwater inflow of similar composition, an inhibited P-cycle in LPM due to meromixis should be the major reason for the overall higher Si consumption in the lake water of LGM. Additionally, anthropogenic P and N influx from numerous recreation facilities at the eastern bank of LGM is certainly responsible for the relatively higher Si uptake in the modern LGM. Water profiles of late summer 1994 document a substantial NH_4 and SRP reservoir in the anoxic hypolimnion of LGM, which gets seasonally bio-available during overturn. During summer stratification in the year 1994, distinct NH_4 and PO_4 concentration gradients (Fig. 3a, c) sustained a continued upward flux of NH_4 and SRP by turbulent diffusive transport. Nitrogen becomes bio-available by nitrification in the anoxic/oxic transition zone. Since nitrate gets rapidly consumed by primary producers it was not detectable in the analyzed water samples.

There are no implications for incomplete mixing of the LGM water body during overturn by the profile pattern of Ca, Mg, Na, K and Cl (Figs. 2c, d; 3d–f). The obtained slight concentration increase of Na, K and Cl in the epilimnion is related to evaporation from the lake surface at strong thermal stratification of the upper 10 m water column (Fig. 2a, b). Heavy rainfall between 23 August and 18 September reset the enhanced Na, K and Cl concentrations of the epilimnion by dilution. The lake obviously received substantial groundwater inflow fed by percolation of the rain. Hydrochemical profile data document enhanced subsurface inflow of low-Mg water at two depth levels (Fig. 2d). The groundwater inflow was obviously less mineralized than the lake water and contained sufficient oxygen for

a nearly quantitative precipitation of Fe; whereas Mn, which is not as sensitive to oxidation as Fe, showed no variation (Fig. 3g, h). The profile of SRP does not document co-precipitation of PO_4 with settling Fe(III)-precipitates. Instead SRP further increased between 23 August and 18 September (Fig. 3a). During summer stratification, the SO_4 concentration had significantly decreased in the anoxic deep water, but increased again by the inflow of groundwater (Fig. 3i). The SO_4 concentration of the deep water is a major parameter that determines the molecular diffusive flux of SO_4 into the sediments, where it is used as an electron acceptor for anaerobic bacterial respiration and microbial mediated anaerobic oxidation of methane (e.g. Furrer and Wehrli *1996*; Iversen and Jørgensen *1985* and references therein). Hydrogen sulphide produced by SO_4 reduction releases PO_4 from its precipitates with Fe. Inflow of SO_4-bearing groundwater may therefore indirectly influence the P-cycle of LGM. It directly affects the nutrient availability in the phototrophic zone of the lake during stratification by additional upward advective nutrient transport. The increase in the dissolved salt concentration (DSC) in the deep water of LGM at the end of the summer stratification in 1994 was relatively minor (Fig. 3j). Increase of DSC is largely contributed to by diffusive reflux from the surface sediments and dissolution or microbial mediated degradation of settling biogenic matter, respectively (Ca, DIC, NH_4, Si, PO_4, Fe, Mn). In the modern dimictic lake, the inventory of these dissolved components is seasonally reduced by biogenic uptake or chemical precipitation and cannot accumulate at a multi-annual scale. The LGM lake water is moderately mineralized, so we could not obtain hints for subsurface inflow of highly saline waters that could trigger development of meromictic conditions. Temporary enhanced groundwater inflow associated with a rainy period in late summer 1994 was slightly less mineralized than the lake water.

Solid sediments

Radiometric data

Unsupported ^{210}Pb in the upper 15 cm of the LPM core and in the LGM core from 4 m depth shows similar high activity values and a distinct decline in the upper sections of these cores (Fig. 4a–d, Table 1). The activity of unsupported ^{210}Pb in the top of the 23 m LGM core is distinctly lower than that of the LPM sediments and of the 4 m core from LGM. In the 55.5 cm long LGM record from 23 m, unsupported ^{210}Pb activities scatter around 300 mBq/g and do not show a systematic decrease with depth. The latter reflects relatively higher sediment accumulation at the centre of the lake basin due to focussing of the settling particle flux towards the profundal which particularly affects micro-sized particles. Associated higher dilution of unsupported ^{210}Pb may be partially counterbalanced by fractionation of the settling particle flux since atmospheric ^{210}Pb shows a high affinity for micro-sized dust particles. The ^{137}Cs profiles confirm that sediment accumulation at the 23 m site distinctly exceeds that of the profundal LPM sediments and that of LGM sediments from the shallow water (Fig. 4e–h). In deeper sections of LGM cores from 4 m and 6 m and of the LPM core, ^{137}Cs could not be detected. These cores clearly cover sedimentation before the beginning of atmospheric nuclear weapon tests which is not the case for the 23 m core. Sediment samples of LGM with significant ^{137}Cs contamination show 50–100 mBq/g higher ^{137}Cs activities than related sediments from LPM. The latter implies ^{137}Cs release from the surface sediments of the meromictic LPM by $^{137}Cs/NH_4$-exchange (e.g. Comans et al. *1989*) or lower ^{137}Cs influx from the LPM catchment which appears unlikely as the only explanation. Export of ^{137}Cs in dissolved form from LPM into LGM may contribute to the relative ^{137}Cs excess in the LGM sediments.

Unsupported ^{210}Pb is exponentially declining in the upper 37.5 cm of the 4 m core (Insert, Fig. 4a). In the lower core section (31.5–55.5 cm) of the 4 m profile, however, unsupported ^{210}Pb values vary between 38 and 69 mBq/g without showing a declining trend versus depth. The latter implies physical mixing by bio-turbation, gas release and/or disturbances during sampling. The mean mass accumulation for the upper 37.5 cm of the 4 m core, calculated on the basis of CIC model assumptions (Appleby *2001* and references therein) and assumed data for porosity and mean density of the solid sediment (Table 1), accounts for 0.081 g/cm^2 yr. Activity values of sediments between 1.5 and 7.5 cm are relatively enhanced versus adjoining deeper samples which may reflect improved scavenging of ^{210}Pb in the shallow water area by increased deposition of planktonic matter. The initial unsupported ^{210}Pb activity of 760 mBq/g calculated on the basis of CIC assumptions probably exceeds that of earlier sedimentation periods. The latter results in too old age values, particularly for the sediment section between 13.5 and 19.5 cm.

In the 6 m core, unsupported ^{210}Pb declines nearly to zero. We applied the CRS-approach assuming various depth values between 16.5 and 25.5 cm for the ^{137}Cs-chronomarker 1963. Unfortunately, no unsupported ^{210}Pb data are available for the upper 6 cm sediment. The plausibility of the inferred chronologies, however, was verifiable by the calculated ages of the 7.5 cm sample. A mean sedimentation rate (cm/yr) close or above those of the 7.5 and 10.5 cm samples had to result for the upper 6 cm sediment. A plausible radiometric chronology could be derived assuming a depth of 21.5 cm for the year 1963 (Table 1). The corresponding constant flux of unsupported ^{210}Pb at the 6 m core site for this assumption is 481 Bq/m² yr. The flux rate estimate falls above the local atmospheric flux range for unsupported ^{210}Pb (50–150 Bq/m² yr) after Preiss et al. (*1996*). The high elevation of the study site may favour wash-out of atmospheric ^{210}Pb by wet deposition and the lake may receive additional influx of unsupported ^{210}Pb via surface run-off from the interior of the crater.

Geochemical and mineralogical sediment composition

In the following section, we will qualitatively investigate spatial and temporal variations in the composition of LGM sediments with reference to sediments from the meromictic LPM. On the basis of bulk geochemical data, we intend to elucidate: (1) possible variations in the balance between planktonic and macrophytic organic matter and in the net accumulation of autochthonous calcite along the transect from the littoral zone to the profundal, (2) the balance between autochthonous organic matter and the allochthonous minerogenic sediment fraction for various depth sections, (3) possible fractionation of the mineral influx within the lake basin, (4) sedimentary implications for dissolved element influx by groundwater inflow and (5) the importance of sediments from various depth sections for the P- and S-cycle in LGM.

(1) LGM sediments from the coring sites at 23, 6 and 4 m document TOC/N increase from the profundal to the littoral zone, which reflects increasing contributions of non-planktonic matter in the shallow parts of the lake (Fig. 5a). The TOC/N values of the 4, 6 and 8 m cores decline in their upper sections close to the TOC/N ratio of the profundal sediments (~10). This reflects increasing contributions from planktonic matter for the shallow water sediments as a result of eutrophication. TOC/N peaks obtained in the 4 m core may reflect temporal expansion of submerged vegetation; however, we do not have independent evidence for it. Relatively higher TOC/N ratios in sediments from the steeply inclining part of the lake basin (8 m core), particularly in sediments between 25 cm and 45 cm where TOC shows a distinct decrease (Fig. 5b), may reflect preferential accumulation of larger and heavier terrestrial plant

remains and/or document prevailing of residual organic matter at an overall much higher degradation degree of the initial organic deposit. We cannot favour one of these explanations on the basis of bulk geochemical sediment composition alone. Influx of terrestrial organic matter is more significant for the small and less productive LPM. Therefore, the highest TOC/N ratios are obtained in the sediments of this lake.

Sediments of LPM and profundal LGM sediments are nearly non-calcareous, whereas LGM sediments from 4, 6 and 8 m reflect successions from non-calcareous to calcareous sedimentation (Fig. 5c, d). The Ca/Sr profiles show similar variations to those of Ca and CO_3 (Fig. 5c–e). In LGM sediments, Ca/Sr declines between water depths of 4 and 23 m. Ca/Sr ratios of bulk sediments increase for enhanced contributions from low-Sr autochthonous calcite. It could be tempting to correlate the sediment cores from 4 and 6 m based on the distinct $CaCO_3$ increase in both records. Radiometric data of the cores (cf. Figs. 4e, f; 5c–e), however, do not allow such a correlation. In our interpretation, CO_3 increase in the shallow water sediments reflects the most recent sedimentation history at an overall higher photosynthetic production rate in the littoral and sub-littoral zone of the lake. Diurnal increase of pH by CO_2-uptake for primary production and significant warming of the epilimnion during summer stratification triggers the precipitation of lake marls by $CaCO_3$ over-saturation. The enhanced carbonate contents, particularly in the 4 m core, may represent substantial portions of calcite incrustations from submerged aquatic vegetation. The settling flux of autochthonous calcite particles also increased for the deep water zone by eutrophication. A sufficient CO_2 reservoir in the deep water fed by CO_2 release during aerobic decomposition of settling organic matter, possibly combined with subsurface inflow of CO_2-containing fluids, maintain a sufficient dissolution rate of the $CaCO_3$ flux to sustain nearly non-calcareous sedimentation at a water depth of 23 m.

(2) Allochthonous minerogenic sediment components (All_{inorg}) and organic matter of LGM sediments experience variable dilution by autochthonous calcite (Fig. 5c, d). Figure 5f shows estimates of the bulk siliciclastic sediment fraction (All_{inorg}) on a $CaCO_3$-free basis as derived from Al concentration data (Fig. 5g). Negligible contributions from further authigenic mineral precipitates and constant All_{inorg} composition with 15.6 wt% Al_2O_3 are assumed for this estimation (Al_2O_3 content for mean continental crust composition, Taylor *1964*). If we consider TOC and N contents, biogenic opal accounts for approximately 50 wt% in the nearly non-calcareous sediments from the 23 m site. Such high values were analytically determined in pre-industrial Holocene sediments recovered from a water depth of 6 m (Robinson *1994*).

The balance between All_{inorg} and autochthonous biogenic matter (biogenic silica + organic matter) for the upper 12 cm of the 6 m core is roughly the same as that for the 23 m sediments. The All_{inorg} decrease in deeper sediments of the 6 m core can be convincingly explained by higher dilution through non-planktonic organic matter (cf. TOC and TOC/N profiles, Fig. 5a, b.) A higher dilution through planktonic organic matter should explain the All_{inorg} decrease in the top sediments of the 4 m core. Peaks of All_{inorg} in the 4 m core around 57 and 36 cm reflect enhanced local soil erosion. According to the ^{137}Cs profile data, sediment accumulation is roughly the same for the 4 and 6 m site. The above estimates document that the balance between allochthonous sedimentation and biogenic deposition varied substantially at the two sites and did not change synchronously. In LGM, settling of fluvial input by surface run-off might be significantly influenced by the occurrence of submerged vegetation in the shallow water area.

(3) The influx of local minerogenic debris that may be transported by surface run-off or near-surface aeolian transport into LGM varies with climate, vegetation dynamics, and human impact. The All_{inorg} fraction of LGM sediments is a complex mixture of local volcanic ejecta, including lithoclastes from the sedimentary basement and aeolian deposits of remote provenance (loess-like components and distal volcanic ashes). Flux rates of conservative major elements are frequently used in paleoenvironmental studies to quantify changes in soil erosion. It cannot be expected that the detrital influx gets equally distributed across the lake bottom. The minerogenic input experiences a dynamic fractionation according to grain size and density, with an overall focussing of the fine particle flux towards the centre of the lake basin. Lake level fluctuations can substantially affect the internal particle fractionation by extension or reduction of the shallow water area of LGM. Initial geochemical signatures of the allochthonous minerogenic sediment constituents can get modulated by chemical alteration and authigenic mineral formation.

Sample preparation for chemical analyses by dry-sieving of the freeze-dried sediments documented the occurrence of dark sandy tephra particles between 0 and 12 cm in the profile from the 8 m sampling site and between 48 and 51 cm in the 6 m core. These particles were largely removed by dry-sieving. Thus, geochemical signatures of these materials find only weak reflection in the shown element profiles. The siliciclastic silt fractions of selected sediment samples from the 6 m site are composed of augite, plagioclase (albite), leucite, orthoclase and quartz (Table 2). Olivine, orthopyroxene and spinel as the major mineral phases of mantel xenoliths in local carbonatites/melilitites of the Monticchio unit are not detectable. While hauyne was not obtained, its occurrence is obvious in local soils by its strikingly blue-coloured mineral particles. Fiore et al. (*1995*) report the occurrence of quartz (3–18%) in weathered igneous rocks of the Vulture volcano. Substantial quartz contents of LGM sediments at the 6 m site may represent quartz from reworked sedimentary rocks of the basement and/or aeolian influx of remote provenience (e.g. Saharan dust).

The Al/Ti ratios of local volcanic rocks show a relatively wide variation range. In all probability, however, Al/Ti of local volcanic debris should be lower than that of remote dust, with a composition close to loess or mean continental crust composition, respectively. We cannot infer general differences between the siliciclastic sediment fractions from the littoral zone to the profundal on the basis of the Al/Ti profiles (Fig. 5h). In the 6 m profile, a distinct Al/Ti-minimum at 16.5 cm coincides with slightly enhanced Al content. A decrease in Al/Ti, Al and All_{inorg} below 50 cm coincides with an increase in TOC, TOC/N (Fig. 5a, b, f–h). Sediments of LPM show overall lower Al/Ti values.

A prominent geochemical signature of the igneous rocks of the Monte Vulture complex including the LGM carbonatite-melilitite formation is the distinct enrichment of light rare earth elements (LREEs), as seen in data presented by De Fino et al. (*1986*) and Stoppa and Principe (*1998*). Chondrite-normalized La concentrations in the igneous rocks from the Vulture complex typically range in the order of 1,000, whereas loess, which may be representative of dust influx from remote source regions, is characterized by a Chondrite-normalized La value of ca. 100. We qualitatively assess possible variations in the provenance of the siliciclastic sediment components by the ratio of Chondrite-normalized La and Tm concentration data (La_N/Tm_N, Fig. 5i, Loess: ca. 9, local volcanic rocks: ca. 100–500). The La_N/Tm_N ratios of LPM sediments generally exceed those of the LGM sediments. This implies a higher proportion of volcanic material of local provenance in the LPM sediments, which is also indicated by the Al/Ti difference between LGM and LPM sediments. LGM

sediments from 4 and 23 m show relatively constant La_N/Tm_N values around 30. The La_N/Tm_N profile from the 6 m sampling site reflects changes in the composition of the siliciclastic sediment constituent in its deeper section. Lowered La_N/Tm_N values below 30 cm coincide with distinctly lowered Al_{inorg} concentrations. Minor Al-maxima around 16.5 and 27.5 cm coincide with increased La_N/Tm_N values. The enhanced siliciclastic influx during these sedimentation intervals is obviously of local origin.

The La_N/Tm_N ratios of the 8 m core are also close to 30 for the top sediments, but distinctly decline to 15 in deeper sections. The geochemical signatures of deeper sediments at the 8 m depth, showing distinctly lower Al contents (Fig. 5g), could reflect the presence of minerogenic debris with a geochemical composition that completely differs from those of the other LGM cores. Figure 6a, b demonstrates the deficit of major and minor elements in deeper sections of the 8 m core versus their average contents in the upper 10.5 cm sediment. The balanced element ratios roughly vary around 0.2, with the exception of Fe, Mn and minor elements (V, W, Mo, U, Sb) that form oxy-anions that can be co-precipitated with Fe(Mn)-oxi-hydroxides. Iron and Mn show distinctly lower deficits versus their contents in the top sediment. Uranium is not depleted, while Mo is enriched by a factor of 3. Both elements are known to behave as relatively mobile in oxic aquatic environments. A further peculiarity of the 8 m core is a greater depletion of rare earth elements from heavy to light REEs for sediments below 10.5 cm (Fig. 6c). The latter is more pronounced in two depth sections (16.6–22.5 cm and 28.5–34.5 cm) with distinct Fe/Al, U/Al and Mo/Al peaks (Fig. 5j–l). The contrast in the geochemical signatures cannot be explained by a differing provenance of the siliciclastic influx, it must be generated by fluid/solid interaction.

(4) Lago Grande di Monticchio and LPM represent sinks for dissolved elemental input from groundwater (e.g. Fe, Mn, Mo, U). Balanced net accumulation of the dissolved trace element influx is assessed in paleohydrological studies (e.g. Schettler et al. *1999*). Inflow of groundwater is favoured in those parts of the LGM basin that are not covered substantially with low-permeable lacustrine sediments. This is most likely the case for near marginal sites and for the steeply inclining sections of the LGM and LPM basins. Dissolved influx of Fe^{2+} can precipitate close to its entrance site if it occurs in oxic environments, or it can be distributed over a larger area if it is seasonally precipitated during overturn. Lago Grande di Monticchio received inflow of oxic groundwater into the anoxic hypolimnion after heavy rainfall in the late summer, which may represent specific hydrological conditions for it. Generally, dimictic lakes with prevalent seasonal anoxic conditions in the deep water show a distinct Fe-cycle. Initial Fe(III)-precipitates are microbially reduced in the anoxic profundal sediments and are released into the pore water. Together with the Fe release from chemical alteration of Fe-hosting debris this sustains diffusive reflux of dissolved Fe into the overlying water column. Above a thermodynamically determined threshold, Fe is immobilized by authigenic mineral formation (sulphides, phosphates, carbonates). During overturn, the released Fe^{2+} is re-precipitated together with possibly new, externally dissolved Fe influx from the groundwater inflow.

In the following section, we estimate the resulting net accumulation of authigenic Fe-precipitates (Fe_{exc}) by a geochemical mass balance for various depth sections of LGM. The estimates are based on an assumed constant Fe/Al value of the bulk minerogenic debris. A hypothetical Fe/Al mass ratio of 0.9 gives minimum Fe_{exc} for all LGM sediments except for the lowermost samples of the 6 m site (Fig. 5m). Sediments from 23 m show a constant Fe_{exc} that is the lowest overall. Three mechanisms may explain the lower Fe_{exc} of the profundal

LGM sediments: (i) The dissolved Fe influx into the deep water and possible focussing of the settling FeOOH flux towards the centre of the lake basin does not counterbalance the Fe_{exc} loss by deposition of FeOOH particles in the shallow water area during overturn. (ii) Fe_{exc} deposition in the profundal experiences a higher dilution by allochthonous sedimentation and (iii) sediments from the 4 m and 6 m site receive substantial Fe influx from near-surface groundwater inflow close to the lake margin. Co-precipitation with FeOOH is an important mechanism that can transfer dissolved oxy-anions of U(VI) and Mo(VI) from the water column into the sediments (e.g. Bruno et al. *1995*; Gustafsson *2003*). We apply normalization using the conservative major element Al to indicate the occurrence of associated Mo and U excess in the sediments. In particular, sediments from the 4 m core show Mo/Al and U/Al peaks that coincide with Fe_{exc}-maxima (Fig. 5j–m). Precipitates of FeOOH produced during seasonal overturn should be characterized by a uniform chemical composition. The Mo and U excess peaks of the 4 m core, therefore, should originate from near-marginal Fe, Mo and U influx via groundwater inflow. Sediments from the 8 m site show exceptionally high Fe_{exc}, U/Al and Mo/Al peaks (Fig. 5k–m). Geochemical peculiarities of the 8 m core may reflect ongoing intense chemical alteration, resulting in a similar profile pattern for Mo/Al and U/Al. Inflow of Fe-rich groundwater close to the location of the 8 m core site at the steeply declining section of the LGM basin may contribute to the Fe excess.

The Fe/Al and Mo/Al profile development of LPM sediments distinctly differs from that of the LGM sediments. Coinciding Fe/Al, Mo/Al and S_{total} peaks occurring above 50 cm document enhanced sulphide precipitation of dissolved Fe and associated co-precipitation of Mo (Fig. 5j, l, n). Molybdate is less particle-reactive than U(VI). The deposition of dissolved MoO_4^{2-} is significantly enhanced under anoxic conditions by reaction with H_2S (Vorlicek et al. *2004*; Tribovillard et al. *2004* and references therein). The latter explains why LPM developed to become an efficient sink for Mo with an increase of H_2S generation.
A relationship between sulphate reduction and Fe retention and post-depositional Fe redistribution cannot be excluded for the shallow water sediments of LGM a priori. In cores from 4 and 6 m, peaks of Fe and S_{total} coincide (Fig. 7a, b). The coincidences could document the diffuse flux of H_2S towards sediment sections with higher reactive iron inventory. They may also reflect in situ sulphide precipitation within discrete sulphate reduction zones and the diffusive flux of Fe dissolved in pore water towards these zones. In the second case, Fe_{total} and Fe/Al sediment profiles hardly record changes in the dissolved elemental influx by groundwater inflow. Assuming constant chemical composition of the detrital influx and a constant Fe/Mn ratio of the groundwater inflow, any variations of Fe/Mn sediment profiles may document Fe/Mn fractionation within the aquatic systems of both lakes. Water profiles of LGM indicate that lake internal cycling of Mn and Fe reaches a similar order of magnitude (Fig. 3g, h). Enhanced authigenic sulphide precipitation during the more recent sedimentation history of LPM obviously proceeded in favour of Fe (Fig. 7c). Most recent LGM sediments from 4, 6 and 23 m are characterized by nearly identical Fe/Mn ratios. Deeper sediment sections from the 4 and 6 m sites show minor differences in their Fe/Mn characteristics. There is no significant Fe/Mn excursion in sediment sections with Fe_{total} and S_{total} peaks. If Fe_{total} peaks reflect post-depositional re-distribution of Fe towards discrete sulphate reduction zones, this must have affected Mn in the same manner.

(5) The P_{total} contents of the LGM sediments increase from the shallow water area to the profundal zone, reflecting a relatively higher P reflux from the shallow water sediments. This interpretation is sustained by TOC/P characteristics of LGM sediments from various water depths (Fig. 7d, e). Higher TOC/P values in deeper sections of the 6 m site may reflect higher

contributions from macrophytic plant remains (Figs. 5a, b; 7e). Lake internal P-cycling must be seen in a close context to the S-cycle since H_2S produced during sulphate reduction releases phosphate from its precipitates with Fe. Otherwise, sulphate reduction is associated with alkalinity production (e.g. Gibblin et al. *1990*), which counteracts the release of surface-bound PO_4 (calcite) and PO_4 release by dissolution of hydroxylapatite. We, therefore, briefly examine below, the sulphur contents and the sulphur speciation of LGM sediments from various water depths.

The total sulphur concentrations of shallow water sediments from 4 and 6 m exceed the S_{total} contents of sediments recovered from the 23 m depth (Fig. 5n). Sulphate is utilized as an electron acceptor for the bio-degradation of organic matter in the absence of other preferentially used electron acceptors (O_2, NO_3, reactive Fe(III), e.g. Furrer and Wehrli *1996*) and is consumed by anaerobic methane oxidation (e.g. Iversen and Jørgensen *1985*). The diffusive penetration of oxygen into surface sediments, which depends on the oxygen concentration of the overlying water and the oxygen consumption rate in the sediment (mainly aerobic mineralization of organic matter and oxidation of reduced sulphur), determines the sediment depth where sulphate reduction can principally proceed from a thermodynamic viewpoint. In the case of profundal sediments, these depths show seasonal variability by oxygen consumption in the deep water. For shallow water sediments the potential depth level for sulphate reduction decreases by the seasonal increase of microbial reaction rates due to sediment warming during spring and summer.

An estimation of the degree to which sulphur hypothetically bonds with Fe_{total}, assuming that only pyrite is present and that no organic-bound or elemental sulphur exists, shows that sulphide-bound Fe in the shallow water sediments of LGM is relatively more important in the LPM sediments (Fig. 8a). Oxidation of the H_2S released in the course of SO_4-reduction and seasonal re-oxidation of authigenic sulphides often only proceeds to elemental sulphur. Elemental sulphur seems to play a key role in the formation of pyrite, which is less sensitive to oxidation (unpublished personal experimental results). The percentages of elemental sulphur in the total sulphur contents decrease from the profundal to the littoral zone, where sulphate reduction proceeds with pronounced seasonal dynamics. It is likely that these dynamics favour a more effective formation of pyrite.

Much more elemental sulphur was found in an upper sequence of the LPM sediments than in the LGM sediments. With respect to the percentage of elemental sulphur in the total sulphur content, the profundal sediments of LPM are different. More than 50% of S_{total} was specified as elemental sulphur in the top sediments (Fig. 8c). However, it can not be ruled out that sulphur speciation of freeze-dried sediment samples overestimates the real abundance of elemental sulphur in surfaces sediments from a meromictic lake with prevailing permanent anoxic conditions in the deep water. According to personal laboratory experience, S^{2-} is partially oxidized during freeze-drying. Thus, the high elemental sulphur contents may have been present in part as monosulphide-bound sulphur in the fresh wet sediments.

Pore water chemistry

Pore water profiles can be used to assess microbial activity within sediments and the diffusive exchange between sediments and the overlying water. Pore water profiles are subject to seasonal variations. For this reason, they represent the current state of the sediment as a result of previous, often microbially mediated, reactions. One has to be clear that interstitial water

ion-activities are as much in thermodynamic balance with the various precipitates as ion-exchange sites ($K_D = c_s/c_l$) of the sediment particles, and therefore, incompletely represent the mobile ion inventory. Pore water sampling by in situ dialysis techniques is the best way to obtain an unaltered picture of pore water chemistry. Depending on the depth of the single dialysis chamber, a certain time is necessary for equilibration of the ion concentration within the chamber with the interstitial water. During the exposure of the dialysis cell, changes in interstitial water chemistry can occur, which is why in situ dialysis pore water profiles detected in this manner give an integral picture over the exposure time of the dialysis cells.

Calcium and DIC are major contributors to the total DSC of the pore water at all sampling sites. Pore water concentrations of Ca close to the sediment water interface slightly exceed the concentrations of lake water dissolved Ca and are nearly identical for sampling sites at 4, 6, 8, 12 and 23 m (Figs. 2c, 9a). The Ca pore water record from 23 m shows a minor peak close to the sediment water interface, and DIC is enhanced over a larger section below the sediment surface at the 23 m site, which might be related to higher CO_2 release by microbial activity in the top sediments. Otherwise, the enhanced pore water DIC concentrations obtained in the top sediments closely correspond to the DIC concentration level of LGM lake water at a water depth of 23 m from 22 August. The DIC profile pattern, therefore, could also reflect diffusive DIC flux across the sediment/water boundary into the sediment. The pore water profile of the 12 m site is characterized by overall higher Ca and DIC concentrations and shows a distinct decline of the concentration gradients between 35 cm and the sediment water interface. Depending on the amount of autochthonous calcite, different Ca/Sr ratios were determined in the surface sediments: 140 for calcareous sediments at a water depth of 4 m, <40 for non-calcareous sediments from a water depth of 23 m (Fig. 5e). The Ca/Sr ratios of the pore water profiles from various water depths are much more uniform (ca. 70–80) and closely correspond with the Ca/Sr characteristics of the lake water below 5 m (Figs. 2e, 9d). The relatively low Ca/Sr values found in the pore water were surprising, since pore water dissolved Ca and Sr were assumed to originate largely from the post-depositional dissolution of autochthonous calcite characterized by Ca/Sr ratios distinctly above 80. Incongruent $CaCO_3$ dissolution (McGillen and Fairchild *2005* and references therein) associated with preferential Sr release into the pore water provides a principle explanation for the Sr excess in the pore water versus autochthonous calcite composition in the LGM sediments. Sediments from 23 m, however, are nearly non-calcareous. The Ca and Sr inventory of these sediments gets almost quantitatively released into the interstitial water. Presuming a substantial deposition and dissolution of autochthonous calcite for the centre of the lake basin, the diffuse Ca, Sr exchange rates across the sediment/water interface seem to be high enough to maintain pore water Ca and Ca/Sr values close to lake water composition.

The importance of sediments from various depth sections might also be quite different in terms of the lake's internal nutrient cycle. Post-depositional dissolution of biogenic silica depends on pore water pH. Interstitial waters from the nearly non-calcareous profundal LGM sediments are more sensitive to pH decrease by microbial release of CO_2 or possible acidity production in the course of sulphide oxidation than calcareous sediment from the littoral and sub-littoral zone. Release of nutrients from surface sediments into the overlying lake water is rapidly uptaken in the shallow water, which can principally sustain high concentration gradients of pore water dissolved nutrients towards the sediment/water interface. In contrast, gradual accumulation of lake water dissolved SiO_2, NH_4 and PO_4 in the hypolimnion during the stratification periods will result in a flattening of pore water concentrations gradients across the sediment/water boundary or even sustain diffusive nutrient flux into profundal

sediments. Diffusive nutrient exchange across the sediment/water interface is further influenced by a complex of interacting parameters including, e.g. temperature, oxygen availability, vertical and temporal variations in H_2S production by SO_4 reduction, abundance of bio-degradable organic matter, PO_4 retention or release associated with authigenic mineral formation.

Silica pore water concentrations at all depth levels exceed the corresponding SiO_2 concentration in the water profile (Figs. 3b, 8a). Diffusive SiO_2 reflux from the surface sediments into the overlying water, therefore, can proceed at all depth levels. The highest concentration gradients at the sediment/water interface occur in the shallow water area. In LGM, silica pore water concentrations equilibrate at 42 ± 2 mg/l SiO_2 at some distance from the sediment/water interface. The SiO_2 pore water profiles from 23 and 32 m show slight broad maxima around 20 cm. A distinctly declining SiO_2 concentration gradient towards the sediment/water interface was only obtained at water depth of 12 m. This may reflect (i) enhanced advection at this site, (ii) inhibition of the diffusive silica reflux from the surface sediments by bio-film development at the other sites or (iii) insufficient compensation of the diffusive silica loss into the overlying water column by dissolution of biogenic silica. Divers have found that the surface sediments at the 12 m sampling site are less organic and sandier than elsewhere.

Ammonium is the second major cation contributor to the total DSC of the pore water in the surface sediments of LGM. Similar to Ca, it affects the pore water profiles of other ions by occupying cation exchange sites at the solid sediment. High NH_4 concentrations measured in the anoxic deep water of LGM can be sustained by the diffusive NH_4 reflux from the surface sediments (Figs. 3c, 10b). Ammonium is released by anaerobic mineralization of the organic deposit. The NH_4 released is transformed to a bio-available nitrate by seasonal succession between anoxic and oxic conditions. The latter can be transformed into N_2 by denitrification after return to anoxic conditions. The pore water profiles recovered from 4, 6 and 8 m, which show slightly decreasing gradients towards the sediment/water interface, are characterized by generally lower NH_4 concentrations (15–30 mg/l) than the profiles from deeper parts of the lake basin. Ammonium pore water profiles from 23 to 32 m show an opposite trend with high NH_4 concentration values in the upper part. The NH_4 concentration difference between pore water and lake water is 72 mg/l at 23 m and 28 mg/l at 32 m. Ammonium concentration gradients towards the overlying water column should principally force a high NH_4 reflux into the deep water. The obtained pattern of the NH_4 pore water profiles from the centre of the lake basin imply that the NH_4 release rate by anaerobic decomposition of biogenic matter in the sediment top exceeds that of deeper sediments. They document that the NH_4 reflux from LGM sediments at 23 m exceeds those of sediments from the deepest part of the lake (32 m). This finding is reflected in the NH_4 lake water profile (Fig. 3c). The NH_4 pore water profile recovered from the 12 m depth shows a different pattern with a maximum at 42 cm and a concentration gradient towards the sediment/water boundary. The overall highest NH_4 pore water concentration values were measured at the 12 and 23 m sampling site. Distinctly lower concentrations were obtained in the sediments from the 32 m depth. In our interpretation, this reflects different contents of anaerobically metabolizable organic matter within the lake basin. A longer duration of seasonal oxic conditions at the 12 and 23 m sites is associated with the production of larger amounts of bio-degradable organic matter by re-oxidation processes. Generally lower NH_4 concentrations in the pore water of the shallow water sediments reflect extensive seasonal re-penetration of oxygen into the shallow water sediments and associated oxidation of NH_4 in company with high diffusive reflux into the permanently NH_4-depleted epilimnion.

The measurement of SRP in small volumes of pore water is amongst the most unsatisfactory analytical tasks. Within samples with high DIC contents, carbonates can precipitate due to the release of CO_2 and phosphate may be removed by sorption onto these precipitates. Pore water samples with elevated Fe^{2+} contents have a tendency to precipitate Fe-oxihydroxides that can co-precipitate phosphate. For these reasons SRP concentrations of deeper sediment sequences, where higher Fe concentrations occurred in the pore water, are not considered here.

Interstitial water concentrations of SRP at all sampling sites force a diffusive P flux from the sediments into the overlying water column. The SRP pore water profiles largely reflect the displacement of phosphate from its precipitates with iron by reaction with H_2S. There is no simple correlation between H_2S generation and phosphate release into the pore water. The phosphorus released may co-precipitate with carbonate by associated production of alkalinity. During field studies in another lake (Lake Breitling, Germany), we observed that H_2S generated was rapidly oxidized by Fe(III)-precipitates, whilst Fe and phosphate pore water concentrations remained largely unchanged (Schettler *1995*). The sediment response to sulphate reduction, therefore, depends on the extent of oxidation of the surface sediments during the circulation periods, particularly during winter, and on their reactive Fe contents. Only the SO_4 pore water profile from 4 m gives a direct impression of the seasonal diffusive sulphate penetration into the surface sediments of LGM. The SRP pore water profile reflects well the different phosphorus release at various depth levels. More phosphate was released at a depth of 20 cm and was related to a longer duration of H_2S generation. At 8 cm, the phosphate release was associated with the discrete SO_4 reduction at this depth that developed some time later when O_2 penetration in the surface sediments had declined.

At 6 m water depth, the sulphate inventory of the interstitial water was more or less completely consumed until August/September 1994. The accumulative diffusive SO_4 flux into deeper sediment sequences is thus presumed to be lower than at the 4 m site, whereas total H_2S generation within the upper sediments may have exceeded that in sediments from 4 m water depth. Really, SRP interstitial water concentrations in the uppermost 15 cm sediment at 6 m water depth are higher than at the 4 m site.

At a water depth of 8 m, the lowest SRP concentrations in the interstitial water were detected. The diffusive oxygen penetration depth during re-oxidation of surface sediments should be higher at this site because the sediments within the steeply sloping lake basin should have less bio-degradable organic matter. Also, higher oxygen contents in the overlying water should be sustained longer than in deeper parts of the lake. Thus more Fe(III) should be generated during seasonal re-oxidation. The reactive Fe(III) content appears to be high enough to prevent remobilization of PO_4 from its Fe-precipitates below a sediment depth of 8 cm.

The SRP pore water profile at 12 m shows a very different pattern with a maximum at a sediment depth of 10 cm and a strong gradient to the sediment/water interface, similar to some cation profiles at this site. Lowering of the pH seems to be sufficient to prevent precipitation of Ca and Mn, which show elevated concentrations in the pore water at the 12 m site. The highest SRP pore water concentrations were obtained in the surface sediments at a water depth of 23 m, where the NH_4 pore water concentrations also reached maximum values within the LGM basin. Concentrations of SRP and NH_4 in the top of the recovered pore water profiles from 32 m depth reach half of the concentration values obtained at the 23 m sampling site. During August/September 1994, sulphate reduction only proceeded at the sediment/water interface. There is no reason to assume that more H_2S was generated here than at the other sampling sites.

Major components of local debris that may contribute to the allochthonous sedimentation of LGM via surface run-off or near surface aeolian transport are easily weatherable volcanic products from the interior of the LGM crater. Chemical alteration of the debris is favoured in organic sediments with pore waters being rich in dissolved organic molecules. Besides groundwater inflow, post-depositional ion release from this debris, in particular release of mono- and divalent cations and silica may significantly contribute to the DSC of the lake water.

Natrium, K and Mg pore water concentrations closely correspond with their concentrations in the lake water (Figs. 2d, 3d, e, 11a1–c1). A slightly elevated concentration may reflect cation release by chemical alteration combined with elution from solid sediment sorption sites by cation exchange with Ca and NH_4. The pore water profiles from 12 m are exceptional. They adjust at lake water concentrations close to the sediment/water interface and show distinctly increasing concentrations towards deeper sediments far above the lake water concentrations (Fig. 11a2–c2). The concentration gradients sustain diffusive reflux of Na, K and Mg into the lake at this depth section of the LGM basin. It remains unclear if the peculiarity of the 12 m site reflects the escape of mineralized groundwater in the steeply inclining part of the lake basin, or is authigenic in character and documents specific conditions favouring high cation release rates by chemical alteration. At the 12 m site, pore water profiles of Ba and Mn show broad maxima around 30 cm (Fig. 11d2, e2), as it is also obtained for Ca and Sr (Fig. 9a, b). It is likely that lower pH values associated with relatively higher CO_2 activities around 30 cm sustain the enhanced Ca, Sr, Mn and Ba concentrations in equilibrium with authigenic carbonates. Decrease of pH in the calcareous sediments of the shallow water area is well buffered by $CaCO_3$ dissolution. In the nearly non-calcareous sediments from deeper parts of the lake basin, seasonal production of alkalinity associated with sulphate reduction is important. Enhanced CO_2 concentrations in the deep water combined with reduced alkalinity production by seasonal SO_4 exhaustion in the deep water may explain the distinctly higher pore water concentration values for Ba and Fe in the sediments from the 32 m site (Fig. 11d1, f2).

Organic sediment characteristics inferred by Rock-Eval analysis

Data presented in the above sections reflect (i) different sediment accumulation and sediment characteristics for LPM and LGM, (ii) various sediment accumulation and differing balances between planktonic and non-planktonic deposits are documented for LGM sediments themselves and (iii) hydrochemical water profiles and pore water profiles from LGM imply that microbial mediated early diagenetic reactions go on in the surface sediments with distinctly different seasonal dynamics at various depth levels of the LGM basin. One could suppose that associated variations in the degradation of the organic sediment constituents are reflected in basic RE parameters, such as OI and HI. In order to elucidate such possible relationships, individual 3-cm sediment samples from various coring sites were analyzed by applying RE pyrolysis.

The entire set of LGM samples falls within relatively narrow OI and HI variation ranges (Fig. 12a, b), from 100 to 150 mg CO_2 per g TOC and from 370 to 600 mg HC per g TOC for OI and HI, respectively. Deeper (older) LGM sediments from the 4 m site (Table 1, Fig. 4) with low $CaCO_3$ and S_{total} contents (Fig. 5c, d, n), which document an increasing spread of aquatic plants in the shallow water area (cf. TOC/N, Fig. 5a), are characterized by distinctly lower HI and elevated OI values. Eutrophication of LGM seems to be reflected in sediments from the 4 m site by the contrasting trends of OI and HI (Fig. 12a, b). Above 25 cm, LGM

sediments from the 4 m site closely correspond in their OI and HI characteristics with sediments from the other sites. The uppermost sediments of the 6 m sampling site (>10 cm) show increasing HI and decreasing OI values (Fig. 12a, b). Diffusive SO_4 flux into the surface sediments during summer stratification in 1994 was most favoured at the 6 m site. Seasonal re-oxidation of organic matter might be limited by high oxygen consumption for oxidation of reduced sulphur accumulated during summer stratification at the 6 m site of the modern lake. The derived OI and HI data set for LGM sediments does not appear to be sensitive to variable balances between planktonic and non-planktonic organic matter (aquatic plants or terrestrial plant remnants). The TOC/N ratios clearly reflect different contributions from non-planktonic matter, with a declining trend towards the centre of the lake (Fig. 5a). Enhanced TOC/N ratios, however, were also obtained for sediments of the steeply inclining part of the lake basin at water depth of 8 m. This probably reflects low-N refractory organic matter for an overall much higher mineralization extent of the organic debris at this low accumulation site. Sediments of the 8 m site, however, are not distinguishable from other LGM sediments on the basis of their OI and HI values.

RE pyrolysis FID curves of fresh organic matters in stream and lake water particles, recent sediments and soils are commonly characterized by multi-lobed peaks, with the more labile organic fractions belonging to the first half of the pyrolysis curves (Albéric *1998*; Nöel *2001*; Disnar et al. *2003*; Copard et al. *2006*). Figure 13 shows non-normalized pyrolysis heating curves of selected sediment samples from various water depths. The pyrolysis temperature of 400°C is defined as an operational boundary to quantify labile organic components (Disnar et al. *2003*). Sediments of LGM show an overall decrease of the proportions of <400°C pyrolysis products (R400) with depth that documents ongoing post-depositional bio-degradation (Fig. 12c). As expected, the upper range of the R400 parameter is represented by sediments from the 23 m high accumulation site and by the upper sediments from the 6 m site. The lower limit of the R400 variation range is defined by older sediments from the 4 m site. A highly refractory character of sediments from the 8 m site is not sustained by the RE data. Sediments of the smaller LPM show higher TOC/N values than LGM sediments (Fig. 5a). We attribute this to a much higher overall proportion of terrestrial organic matter, particularly, remnants of leaves, blooms and dead wood from the surrounding deciduous forest. Rock-Eval results confirm this interpretation. Hydrogen Index values of LPM sediments are lower overall than those of LGM sediments, whereas OI values of LPM sediments distinctly exceed the OI variation range obtained for LGM sediments (Fig. 12a, b). Because of the permanent absence of oxygen in the LPM deep water, it appears astonishing that OI values of LPM sediments exceed the average OI of LGM sediments by a factor of ~1.5. The relative content in labile organic matter falls below the variation range of LGM sediments (Fig. 12c). In particular, bulk organic matter of deeper LPM sediments shows distinctly lower R400 values. The corresponding sediments are characterized by a more clastic composition (Fig. 5b, g) and document low sulphide precipitation of lake water dissolved Mo (Fig. 5l). Sediments of LPM between 50 and 70 cm can document a former sedimentation interval with enhanced soil erosion. In this case, low HI, high OI and low R400 values can characterize refractory organic substances from local soils that might temporarily become a major component of the bulk organic matter. The relative low maximum water depth of LPM (36 m) does not favour meromixis. Alternatively, the HI, OI and R400 characteristics of deeper LPM sediments may document sedimentation in a low-productivity former dimictic lake with well-oxygenated deep water. We cannot favour one of the two interpretations on the basis of our data set.

Synopsis

(1) Sediments of LGM document gradually increasing contributions from dead planktonic matter in the course of the recent sedimentation history and show clear variations in their geochemical composition depending on water depth. They show TOC/N increase from the profundal to the littoral zone. The carbonate contents of modern sediments decrease towards the centre of the lake basin reflecting lower contributions of littoral calcite and relative higher carbonate dissolution. Changes in the net accumulation of autochthonous carbonate did not proceed synchronously at various water depths. The carbonate profile pattern of LGM sediments from various water depths are therefore not useable as chrono-markers in paleoenvironmental studies. Local igneous rocks are characterized by a distinct enrichment of LREEs. The La_N/Tm_N ratios of the sediments reflect the balance between influx of local debris and aeolian influx of remote provenance (e.g. Saharan dust). Profundal sediments from LGM and LPM do not show significant change of their La_N/Tm_N ratios, whereas LGM sediment cores from the shallow water area document spatial and temporal variations in the influx of local debris. The settling of soil particles from surface runoff into LGM may be highly influenced by submerged vegetation in the shallow water area of LGM. A peculiarity of the Laghi di Monticchio is their relatively high Sr concentration (0.6 mg/l) which is also obtained in springs from the surroundings of the lakes. Autochthonous calcite is characterized by a distinctly higher Ca/Sr ratio than the coexisting lake water. The Ca/Sr profiles of the recovered sediment cores clearly reflect the various contributions from autochthonous carbonate at the individual sampling sites. Assuming a substantial post-depositional dissolution of autochthonous calcite, pore water in the surface sediments should reflect the Ca/Sr signature of the autochthonous calcite. Pore water from all sampling sites, however, showed Ca/Sr ratios close to that of the lake water.

(2) Radiometric data clearly document that sediment accumulation at the centre of the LGM basin is higher than in the shallow water area. The latter reflects substantial focussing of the particle flux towards the centre of the lake basin. Relatively higher accumulation of macrophytic organic remnants and littoral $CaCO_3$ does not counterbalance focussing of the particle flux towards the centre of the lake basin.

(3) At the 4 m sampling site, Fe/Al is slightly enhanced, reflecting near-surface inflow of Fe-bearing groundwater and precipitation of FeOOH in this part of the lake basin. Coinciding U/Al and Mo/Al peaks reflect co-precipitation of U and Mo with these Fe-precipitates. Increase of Fe and Mn in the anoxic deep water by diffusive reflux from the surface sediments, dissolution of settling Fe(Mn)-precipitates and groundwater inflow reaches a similar order of magnitude. The Fe and Mn dissolved in the anoxic deep water are seasonally precipitated during overturn. In summer 1994, the Fe was quantitatively precipitated by the influx of O_2-bearing groundwater after heavy rainfall during summer stratification. The frequency of such events might be detectable by microfacies analysis of sediments from the centre of the lake bottom.

(4) Peaks of Fe_{total} obtained in sediment profiles from the shallow water area coincide with enhanced S_{total} contents. The coincidence could reflect (i) diffusive flux of H_2S towards a sediment section with enhanced reactive Fe content or (ii) diffusive flux of Fe towards a sulphate reduction zone. In the case of coinciding Fe and S_{total} peaks in sediments from 16.5 cm at the 6 m sampling site, overlapping La_N/Tm_N sustains the interpretation (i). We found clear evidence for significant element re-distribution in the sediments of the steeply inclining part of the LGM basin. Seasonal change between anoxic and oxic conditions,

combined with high concentrations of CO_2 and complexing organic acids, may sustain very high alteration rates of volcanic debris. Remobilization of light rare earth elements appears overall higher than that of heavy rare earth elements. Solid sediments from the 8 m site document a significant release of Fe by chemical alteration. Re-precipitation of pore water dissolved Fe as Fe-oxihydroxide is accompanied by substantial co-precipitation of U and Mo. Enhanced chemical alteration in the steeply inclining sector of LGM is documented in pore water profiles from the 12 m site that show distinctly elevated Na, K, Mg, Ca, Mn and DIC concentrations with strong gradients towards the sediment/water interface. Distinctly enhanced Fe/Al and Mo/Al values are also obtained in the upper part of the sediment record from the centre of LPM. In the meromictic LPM, an increase of Mo/Al reflects more efficient deposition of the dissolved Mo influx from the catchment by sulphide precipitation.

(5) Silica pore water concentrations, which should largely originate from the post-depositional dissolution of biogenic opal, have a uniform value of ca. 42 mg/l SiO_2 in LGM sediments. The SiO_2 pore water concentrations obtained principally sustain a diffusive reflux of silica from the surface sediments into the overlying water body in all parts of the LGM basin. Most of the recovered SiO_2 pore water profiles do not show a concentration gradient towards the sediment/water interface. This may document high overall dissolution rates of biogenic opal with declining silica concentrations in the overlying water combined with inhibition of the diffusive flux across the sediment/water interface by bio-film development at the sediment surface. Sediments from the 12 m site are exceptional since they show a clear pore water concentration gradient towards the sediment water interface. During August/September 1994, the lake received diffusive reflux of NH_4 from all sediment sampling sites. As for SiO_2, no NH_4 concentration gradients could be obtained towards the sediment water interface, except sediments from the 12 m site. Enhanced NH_4 pore water concentrations are sustained by anaerobic bio-degradation of organic matter. Individual pore water profiles are influenced by seasonal re-oxidation, which proceeds to a lower extent for sediments from the deepest part of the lake basin. Surprisingly, NH_4 pore water concentrations from the 23 m and the 12 m sites distinctly exceed those from the 32 m site. This implies that regeneration of easily metabolizable organic matter during seasonal overturn is more important for the 12 m and 23 m sites than for LGM sediments from the centre of the lake basin. As for NH_4, the pore water profiles obtained imply that the diffusive reflux of phosphate from the surface sediments is the highest at the 23 m site. Phosphorus availability, which is in principle the limiting factor of pelagic photosynthetic production during summer stratification, however, is sustained at relatively elevated levels by the diffusive reflux of phosphate from surface sediments in the shallow water area. Photosynthetic production in LGM could be characterized by a distinctly more pronounced decline during summer stratification by lake level lowering and the absence of an extended shallow water area.

Acknowledgements

Technical support by two former GFZ-employees, Elke Heilek and Sandra Kostrowski, is acknowledged (laboratory work). Dr Martin Zimmer and Heike Rothe are thanked for ICP-MS measurements, Dr Mathias Gottschalk for XRD-analyses and Andreas Hendrich for support in preparing figures (all GFZ-Potsdam). We thank Prof. Mark Brenner and John P. Smol for editorial handling of the manuscript and two anonymous reviewers who gave valuable hints for improving an earlier draft of the manuscript. We especially acknowledge the risky work in a water-filled dormant volcano by the diving team Uwe Neuman and partner (Potsdam) and thank Dr Claudia Principe (Istituto di Geoscienze e Georisorse, Pisa) for

giving valuable information regarding Monte Vulture volcanism and Prof. J.F.W. Negendank for initiating this study.

References

Albéric P (1998) Transformation of riverine organic matter from sinking stream recharge to spring discharge in a karst aquifer. Mineral Mag 62A:36–37

Allen JRM, Brandt U, Brauer A, Hubberten H-W, Huntley B, Keller J, Kraml M, Mackensen A, Mingram J, Negendank JFW, Nowaczyk NR, Oberhänsli H, Watts WA, Wulf S, Zolitschka B (1999) Rapid environmental changes in southern Europe during the last glacial period. Nature 400:740–743

Allen JRM, Watts WA, Huntley B (2000) Weichselian palynostratigraphy, palaeovegetation and palaeoenvironment; the record from Lago Grande di Monticchio, southern Italy. Quatern Int 73/74:91–100

Allen JM, Watts WA, McGee E, Huntley B (2002) Holocene environmental variability—the record from Lago Grande di Monticchio, Italy. Quatern Int 88:69–80

Appleby PG (2001) Chronostratigraphic techniques in recent sediments. In: Last WM, Smol JP (eds) Tracing environmental change using lake sediments, vol 1: basin analysis, coring, and chronological techniques. Kluwer, Dordrecht, pp 171–202

Barbieri M, Morotti M (2003) Hydrochemistry and strontium isotopes of spring and mineral waters from Monte Vulture volcano, Italy. Appl Geochem 18:117–125

Brandt U, Nowaczyk NR, Ramrath A, Brauer A, Mingram J, Wulf S, Negendank JFW (1999) Palaeomagnetism of Holocene and Late Pleistocene sediments from Lago di Mezzano and Lago Grande di Monticchio (Italy): initial results. Quatern Sci Rev 18:961–976

Brauer A, Mingram J, Frank U, Günter C, Schettler G, Wulf S, Zolitschka B, Negendank JFW (2000) Abrupt environmental oscillations during the Early Weichselian recorded at Lago Grande di Monticchio, southern Italy. Quatern Int 73/74:79–90

Brocchini D, La Volpe L, Laurenzi MA, Principe C (1994) Storia evolutivia del Monte Vulture. Plinius 12:22–26

Bruno J, De Pablo J, Duro L, Figuerola E (1995) Experimental study and modelling of the U(VI)-$Fe(OH)_3$ surface precipitation/co-precipitation equilibria. Geochim Cosmochim Acta 59:4113–4123

Buettner A, Principe C, Villa IM, Brocchini D (2006) Geocronologia ^{39}Ar-^{40}Ar del Monte Vulture. In: Principe C (ed) La geologia del monte Vulture, Regione Basilicata. Finiguerra, Lavello, pp 73–86

Cavarretta G, Lombardi G (1990) Origin of sulphur in the Quaternary perpotassic melts of Italy: evidence from hayne sulphur isotope data. Chem Geol 82:15–20

Chiodini G, Cioni R, Guidi M, Marini L, Principe C, Raco B (1997) Water and gas chemistry of the Lake Piccolo of Monticchio (Mt. Vulture, Italy). Curr Res Volcanic Lakes 10:3–10

Cioni R, Marini L, Raco B (2006) Il Lago Piccolo di Monticchio: geochimíca dei fluidi e valutazione del rischio di eruzione limnica. In: Principe C (ed) La geologia del monte Vulture, Regione Basilicata. Finiguerra, Lavello, pp 171–177

Comans RNJ, Middelburg JJ, Zonderhuis J, Woittiez JRW, De Lange GJ, Das HA, Van Der Weijden CA (1989) Mobilization of radiocaesium in pore water of lake sediments. Nature 339:367–369

Copard Y, Di-Giovanni C, Martaud T, Albéric P, Olivier J-E (2006) Using Rock-Eval 6 pyrolysis for tracking fossil organic carbon in modern environments: implications for the role of erosion and weathering. Earth Surf Proc Land 31:135–153

Creer KM, Morris A (1996) Proxy-climate and geomagnetic palaeointensity records extending back to ca. 75,000 BP derived from sediments cored from Lago Grande di Monticchio, southern Italy. Quatern Sci Rev 15:167–188

Crisci G, De Fino M, La Volpe L, Rapisardi L (1983) Pleistocene ignimbrites of Monte Vulture (Basilicata, Southern Italy). Neues JB Geol P-H 12:731–746

De Fino M, La Volpe L, Peccerillo A, Piccarreta G, Poli G (1986) Petrogenesis of Monte Vulture volcano (Italy): inferences from mineral chemistry, major and trace element data. Contrib Mineral Petrol 92:135–145

Disnar JR, Guillet B, Keravis D, Di-Giovanni C, Sebag D (2003) Soil organic matter (SOM) characterization by Rock-Eval pyrolysis: scope and limitations. Org Geochem 34:327–343

Downes H, Kostoula T, Jones AP, Beard AD, Thirlwall MF, Bodinier J-L (2002) Geochemistry and Sr-Nd isotopic compositions of mantle xenoliths from the Monte Vulture carbonatite-melilitite volcano, central southern Italy. Contrib Mineral Petrol 144:78–92

Espitalié J, Deroo G, Marquis F (1985) La pyrolyse Rock-Eval et ses applications. Rev Inst Fr Petrol 40:563–579

Fiore S, Huertas FJ, Linares J, Piccareta G (1995) Distribution of trace elements in altered pyroclastites from Monte Vulture volcano (southern Italy). Estud Geol 51:119–127

Furrer G, Wehrli B (1996) Microbial reactions, chemical speciation, and multicomponent diffusion in porewaters of a eutrophic lake. Geochim Cosmochim Acta 60:2333–2346

Giannandrea P, La Volpe L, Principe C, Schiattarella M (2004) Carta geologica del Monte Vulture alla scala 1:25.000. Litografia Artistica Cartografica, Firenze

Giannandrea P, La Volpe L, Principe C, Schiattarella M (2006) Unità di Monte Vulture stratigrafiche a limiti inconformi e storia evolutiva del volcano medio-pleistocenico di Monte Vulture (Appennino meridionale, Italia). Boll Soc Geol Ital 125:67–92

Gibblin AE, Likens GE, White D, Howarth RW (1990) Sulfur storage and alkalinity generation in New England lake sediments. Limnol Oceanogr 35:852–869

Gustafsson JP (2003) Modelling molybdate and tungstate adsorption to ferrhydrite. Chem Geol 200:105–115

Hansen RB (1993) Sonar Investigations in the Laghi di Monticchio (Mt. Vulture, Italy). In: Negendank JFW, Zolitschka B (eds) Paleolimnology of European maar lakes. Springer, Berlin, pp 119–128

Huntley B, Watts WA, Allen JRM, Zolitschka B (1999) Palaeoclimate, chronology and vegetation history of the Weichselian Late glacial: comparative analysis of data from three cores at Lago Grande di Monticchio, southern Italy. Quatern Sci Rev 18:945–960

Iversen N, Jørgensen BB (1985) Anaerobic methane oxidation rates at the sulphate-methane transition in marine sediments from Kattegat and Skagerrak (Denmark). Limnol Oceanogr 30:944–955

Jones AP, Kostoula T, Stoppa F, Woolley AR (2000). Petrography and mineral chemistry of mantle xenoliths in a carbonate-rich melilititic tuff from Mt. Vulture volcano, southern Italy. Mineral Mag 64:593–613

Lafargue E, Marquis F, Pillot D (1998) Rock-Eval 6 applications in hydrocarbon exploration, production and soil contamination studies. Rev Inst Fr Petrol 53:421–437

Larson AC, Von Dreele RB (1987) Generalized structure analysis system. Los Alamos National Laboratory Report No. LA-UR-86-748, 224 pp

La Volpe L, Patella D, Rapisardi L, Tramacere A (1984) The evolution of the Monte Vulture volcano (Southern Italy): inferences from volcanological, geological and deep dipole electric sounding data. J Volcanol Geoth Res 22:147–162

Marini L, Chiodini G (1994) The role of carbon dioxide in the carbonate-evaporite geothermal systems of Tuscany and Latium (Italy). Acta Vulcanol 5:95–104

McGillen MR, Fairchild IJ (2005) An experimental study of incongruent dissolution of $CaCO_3$ under analogue glacial conditions. J Glaciol 51:383–390

Möckel HJ (1984) Retention of sulphur and sulphur organics in reversed-phase liquid chromatography. J Chromatogr 317:589–614

Müller H, Frey B, Schweizer B (1992) Grundlagen und Techniken der Fließinjektionsanalyse in der UV-Spektroskopie. Perkin Elmer Druckschrift:B2303.30

Narcisi B (1996) Tephrochronology of a late quaternary lacustrine record from the Monticchio Maar (Vulture Volcano, southern Italy). Quatern Sci Rev 15:155–165

Newton AJ, Dugmore AJ (1993) Tephrochronology of core C from Lago Grande di Monticchio: palaeomagnetism. In: Negendank JFW, Zolitschka B (eds) Paleolimnology of European maar lakes. Springer, Berlin, pp 333–348

Niemistö L (1974) A gravity corer for studies of soft sediments. Merentutkimuslait. Julk/Horsforskingsinst Skr 238:33–38

Nimmergut AP, Allen JRM, Jones VJ, Huntley B, Battarbee RW (1999) Submillenial environmental fluctuations during marine Oxygen Isotope Stage 2: a comparative analysis of diatom and pollen evidence from Lago Grande di Monticchio, South Italy. J Quaternary Sci 14:111–123

Nöel H (2001) Caractérisation et calibration des flux organiques sédimentaires dérivant du bassin versant et de la production aquatique (Annecy, le Petit Lac). Thesis, University of Orléans

Principe C, Stoppa F, Rosatelli G (2006) Modal classification of Monte Vulture volcanics. In: Principe C (ed) La geologia del Monte Vulture, Regione Basilicata. Finiguerra, Lavello, pp 87–103

Preiss N, Mélières M-A, Pourchet M (1996) A compilation of data on lead 210 concentration in surface air and fluxes at the air-surface and water-sediment interface. J Geophys Res-Athos 101:28847–28862

Ramrath A, Zolitschka B, Wulf S, Negendank JFW (1999) Late Pleistocene climatic variations as recorded in two Italian maar lakes (Lago di Mezzano, Lago Grande di Monticchio). Quatern Sci Rev 18:977–992

Robinson C (1994) Lago Grande di Monticchio, southern Italy: a long record of environmental change illustrated by sediment geochemistry. Chem Geol 118:235–254

Schettler G (1995) Dynamik und Bilanz des Schadstoffaustausches zwischen Sediment und Wasserkörper in umweltbelasteten Havelseen. Bericht zum DFG-Projekt Sche/1–2, GeoForschungsZentrum Potsdam

Schettler G, Rein B, Negendank JFW (1999) Geochemical evidence for Holocene palaeodischarge variations in lacustrine records from the Westeifel Volcanic Field, Germany: Schalkenmehrener and Meerfelder Maar. Holocene 9:381–400

Schwedhelm E, Vollmer M, Kersten M (1988) Bestimmung von Konzentrationsgradienten gelöster Schwermetalle an der Sediment/Wasser Grenzfläche mit Hilfe der Dialysetechnik. Z Anal Chem Fresenius 32:756–763

Stoppa F, Principe C (1998) Eruption style and petrology of a new carbonatitic suite from the Mt. Vulture (Southern Italy): the Monticchio Lakes Formation. J Volcanol Geoth Res 80:137–153

Taylor SR (1964) Abundance of chemical elements in the continental crust – a new table. Geochim Cosmochim Acta 28:1273–1285

Taylor SR, McLennan SM (1985) The continental crust: its composition and evolution. Blackwell, Oxford

Tribovillard N, Riboulleau A, Lyons T, Baudin F (2004) Enhanced trapping of molybdenum by sulfurized marine organic matter of marine origin in Mesozoic limestones and shales. Chem Geol 213:385–401

Villa IM (1988) Excess Ar in K-rich volcanites: the role of fluids. Rend SIMP 43:95–104

Vorlicek PT, Kahn MD, Kasuya Y, Helz GR (2004) Capture of molybdenum in pyrite-forming sediments: role of ligand-induced reduction by polysulfides. Geochim Cosmochim Acta 68:547–556

Watts WA (1985) A long pollen record from Laghi di Monticchio, southern Italy: a preliminary account. J Geol Soc London 142:491–499

Watts WA, Allen JRM, Huntley B, (1996a) Vegetation history and palaeoclimate of the last glacial period at Lago Grande di Monticchio, southern Italy. Quatern Sci Rev 15:133–153

Watts WA, Allen JRM, Huntley B, Fritz SC (1996b) Vegetation history and climate of the last 15,000 years at Laghi di Monticchio, southern Italy. Quatern Sci Rev 15:113–132

Watts WA, Allen JRM, Huntley B (2000) Palaeoecology of three interstadial events during oxygen-isotope Stage 3 and 4: lacustrine record from Lago Grande di Monticchio, southern Italy. Palaeogeogr Palaeoclimatol PalaeoEcol 155:83–93

Wulf S, Kraml M, Brauer A, Keller J, Negendank JFW (2004) Tephrochronology of the 100ka lacustrine sediment record of Lago Grande die Monticchio (southern Italy). Quatern Intern 122:7–30

Zolitschka B, Negendank JFW (1993) Lago Grande di Monticchio (southern Italy) A high resolution sedimentary record of the last 70,000 years. In: Negendank JFW, Zolitschka B (eds) Paleolimnology of European maar lakes. Springer, Berlin, pp 278–288

Zolitschka B, Negendank JFW (1996) Sedimentology, Dating and palaeoclimatic interpretation of a 76.3 ka record from Lago Grande di Monticchio, southern Italy. Quatern Sci Rev 15:101–112

Figures

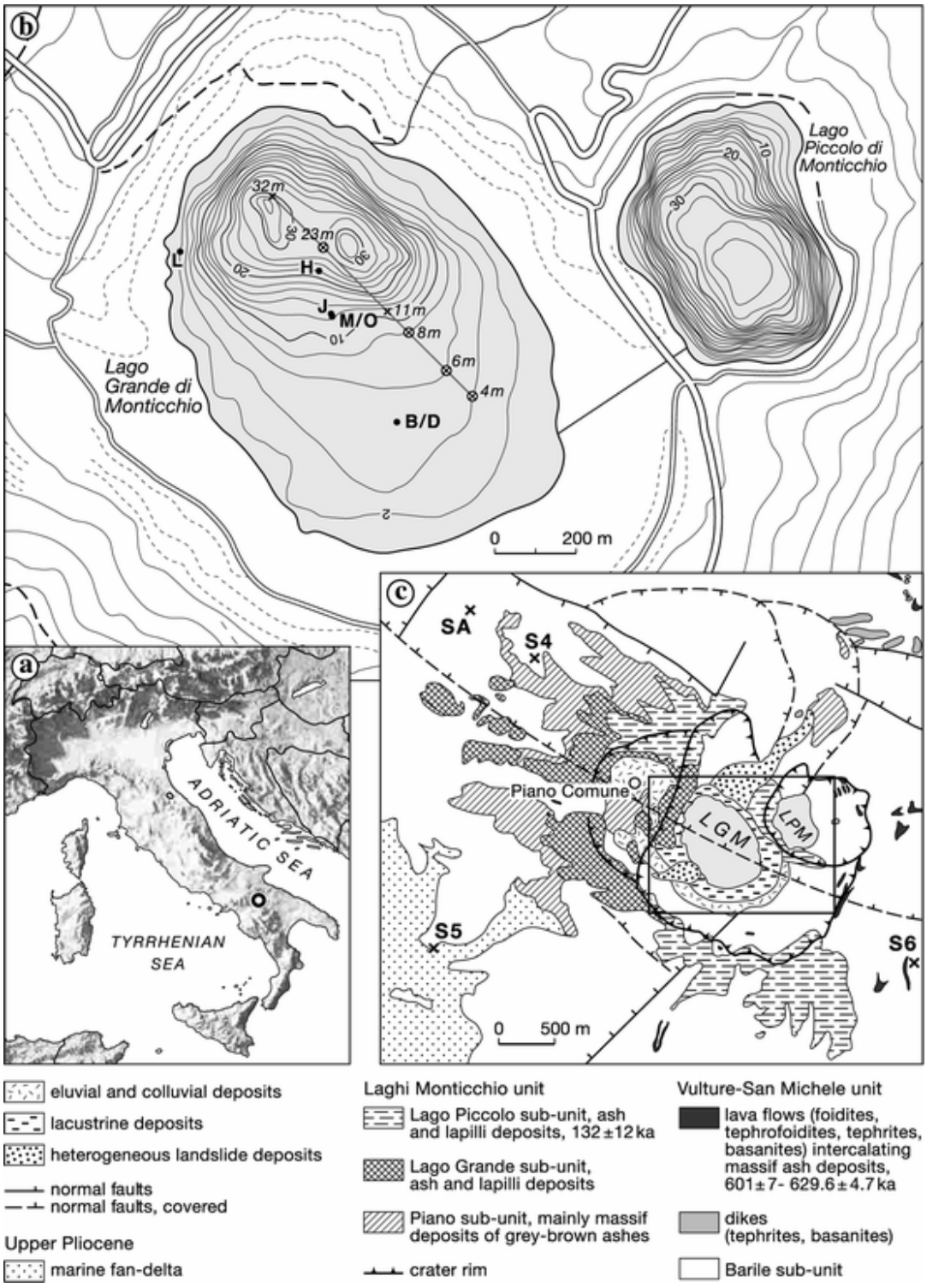

Fig. 1 (**a**) Location of Laghi di Monticchio. (**b**) Bathymetry of the maar lakes, map of Lago Grande di Monticchio showing sampling sites for short cores (○) and in situ pore water profiles (×); locations of piston core records (B, D, J, H, M, O, L) investigated in previous studies are marked inside. (**c**) Geological map re-drawn after Giannandrea et al. (*2004*) showing faults, the crater rim of the Monticchio unit and local springs (SA, S4, S5, S6) analyzed by Barbieri and Morotti (*2003*)

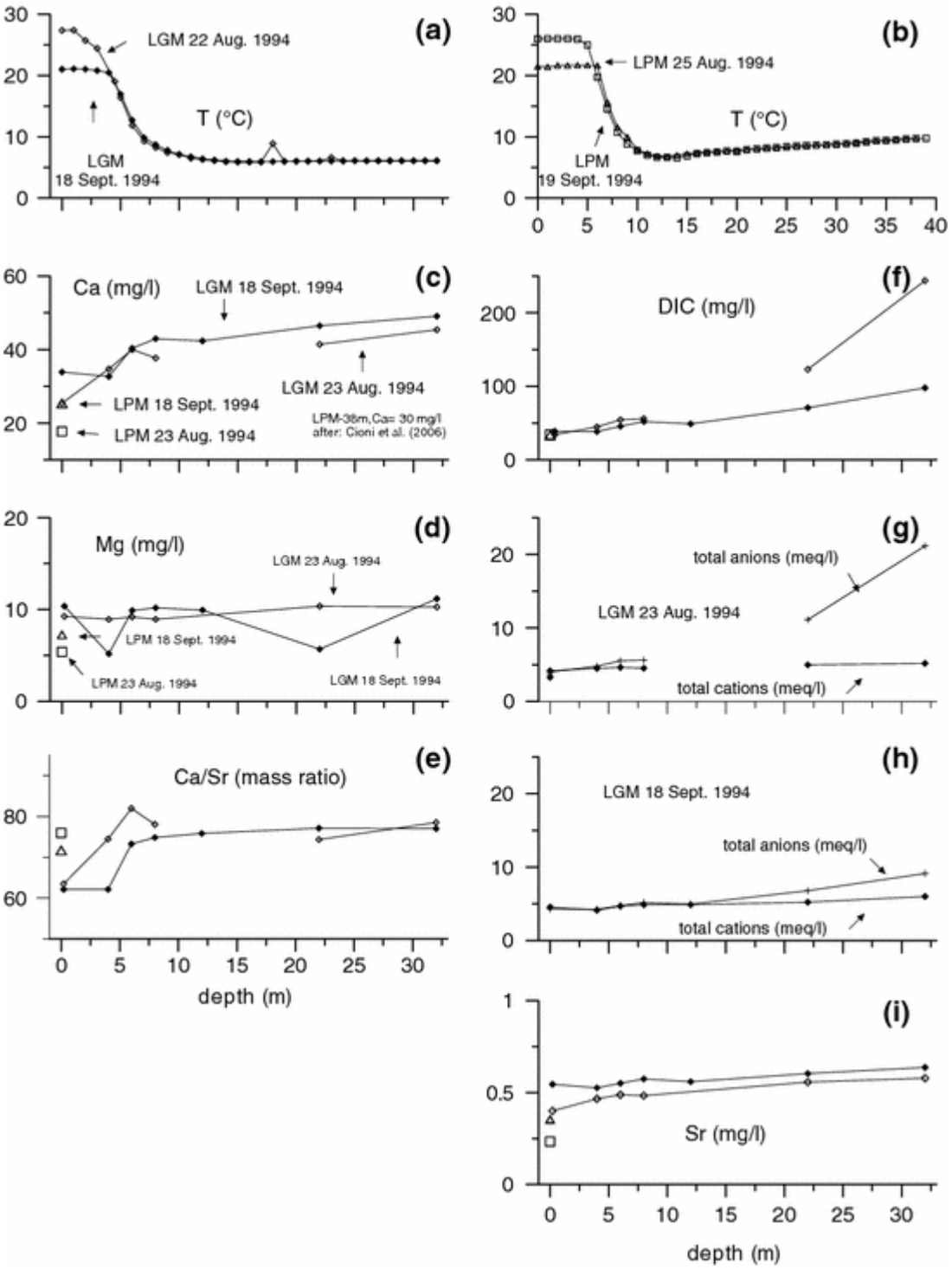

Fig. 2 (**a**, **b**) Thermal stratification of LGM and Lago Piccolo di Monticchio (LPM) in summer 1994. (**c**–**i**) Selected water profiles of LGM for two sampling dates in 1994. Data for surface and deep water composition of LPM are given inside the diagrams for comparison; unique symbols for individual sampling dates are used throughout; data for deep water composition in LPM after Cioni et al. (*2006*) and references therein. Lowered Ca and Ca/Sr values in the surface water of LGM reflect the deposition of low-Sr autochthonous calcite. DIC was considered as HCO_3 for the calculation of anion sums, distinct anion excess, particularly for 22 August, reflects high CO_2 concentrations in the deep water of LGM. High Sr contents are typical for local springs

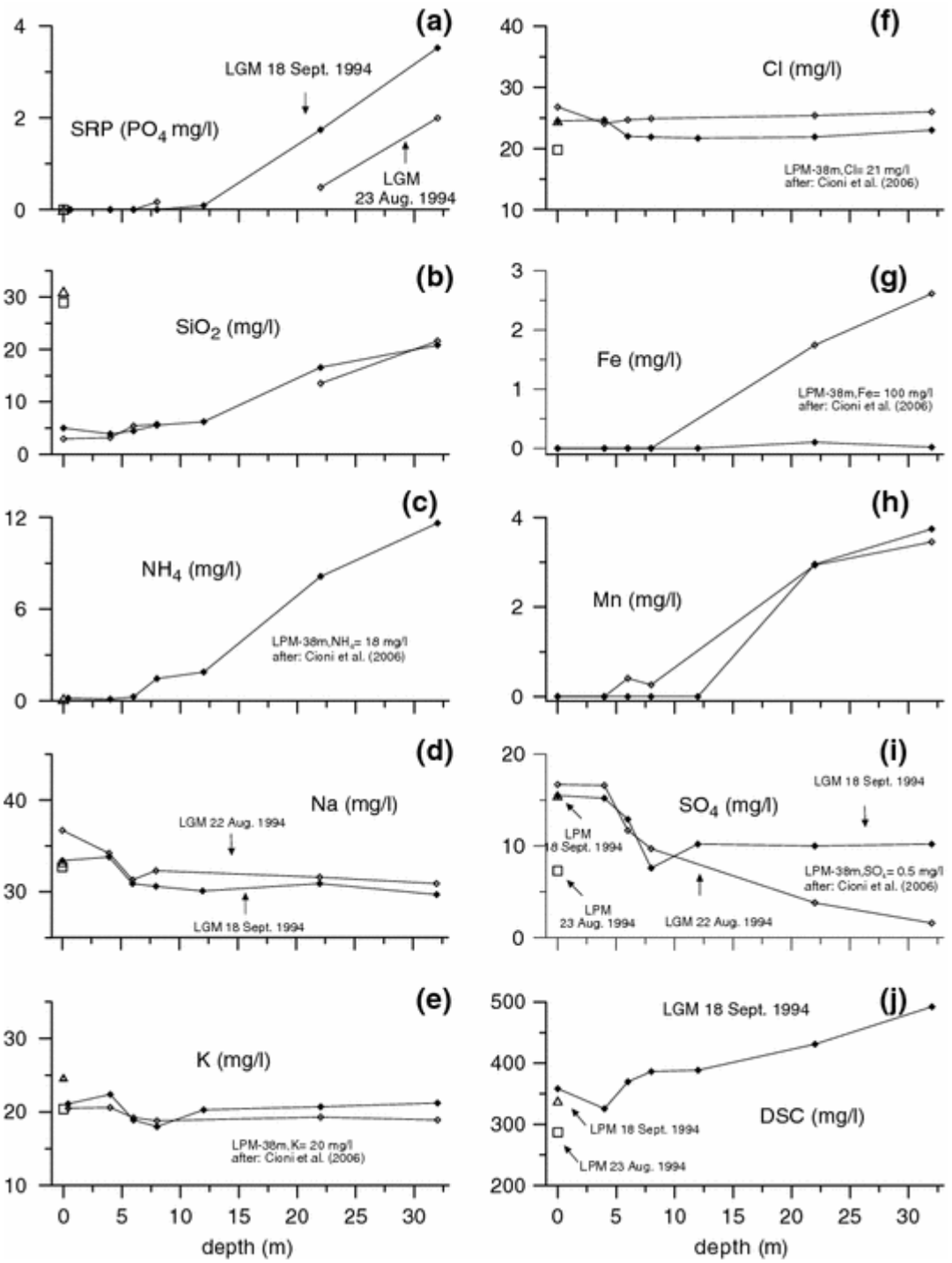

Fig. 3 (**a**–**j**) Selected water profiles demonstrating chemical stratification of LGM for two sampling dates in summer 1994. Data for surface water and deep-water composition of LPM are given inside the diagrams for comparison. Sulphate increase and Fe decrease between 22 August and 18 September 1994 document sub-surface inflow of oxygen-bearing groundwater into LGM, slight Na and Cl increase in the surface water of LGM documents concentration increase due to evaporation. Increase of the Dissolved Salt Content (DSC) in the deep water is mainly contributed by DIC, Ca and NH_4. There are no indications for incomplete seasonal mixing of the LGM water body

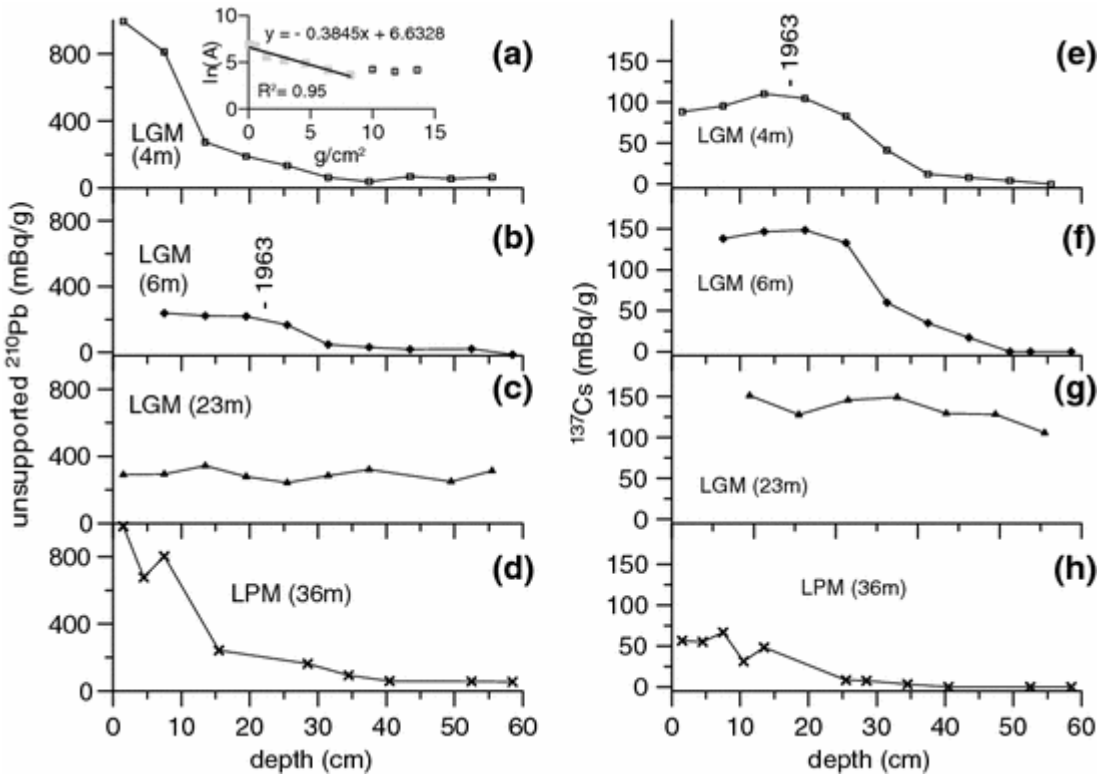

Fig. 4 (**a**–**d**) Unsupported ^{210}Pb and (**e**–**h**) ^{137}Cs profiles of sediment cores recovered in LGM from various water depths along the transect shown in Fig. 1 **b**, and of a sediment core from the centre of LPM. All activity data are given per dry substance and related to 1 September 1994. Insert diagram of (**a**) showing the semi-logarithmic plot of unsupported ^{210}Pb (mBq/g) versus data for cumulative dry mass (m_{cum} in g/cm^2), m_{cum} was calculated on the basis of assumed values for porosity (φ) and density of the solid sediment (ρ_s). Considered φ and ρ_s values and derived radiometric ^{210}Pb-ages for core 4 m, basing on CIC conditions and assumption of constant mass accumulation, are compiled in Table 1; the estimated depth location of the year 1963 is shown in (**e**). The depth estimate for the year 1963 in core 6 m (**b**) was calculated on the basis of CRS assumptions

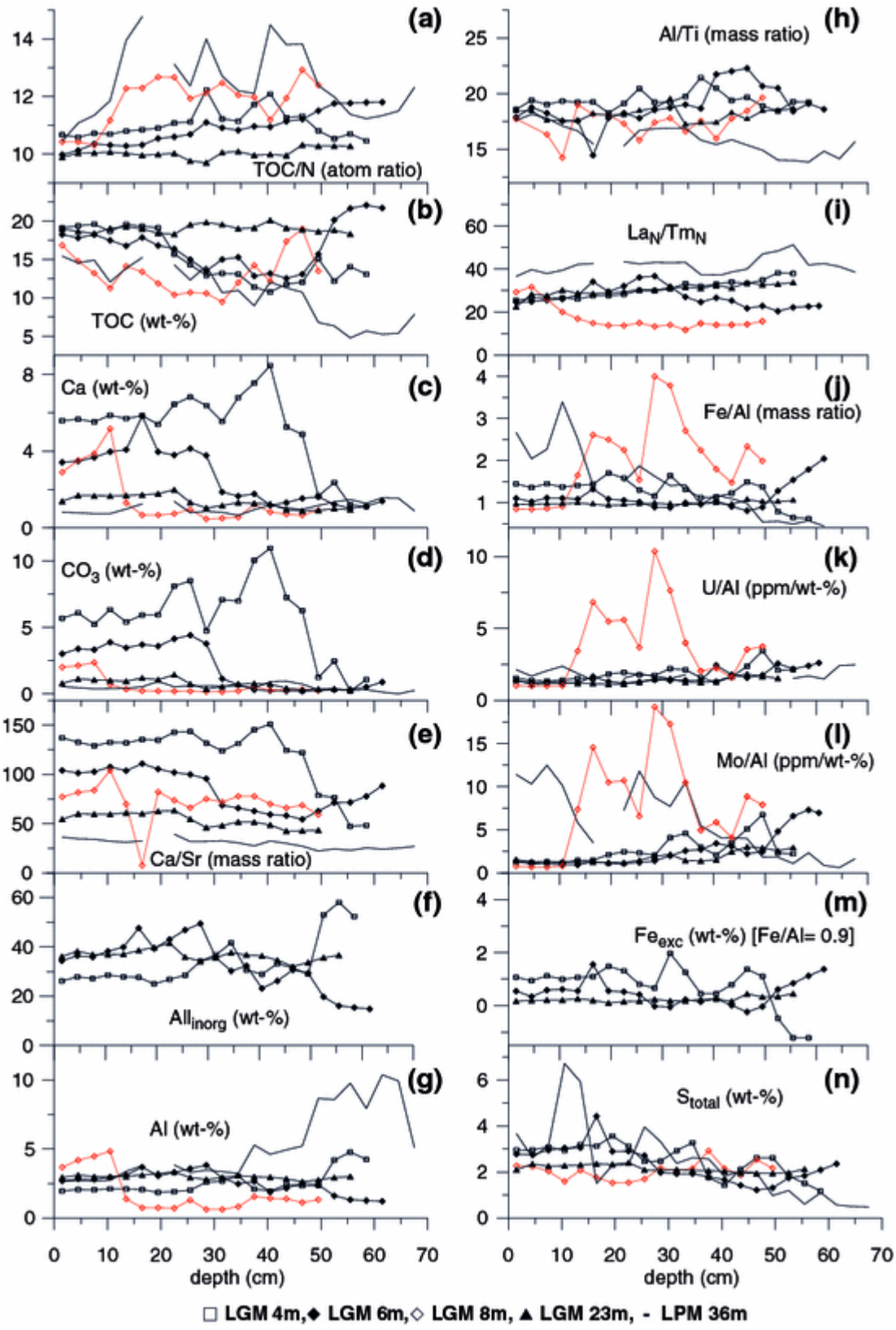

Fig. 5 Selected geochemical sediment profiles of sediment cores from LGM and LPM, respectively, sampling sites are shown in Fig. 1 **b**. Individual data points represent the middle of continuously sampled 3 cm sediment sections. (**a**, **b**) Compilation of TOC/N and TOC profiles demonstrating decreasing contributions of non-planktonic organic matter towards the centre of the lake basin and overall higher contributions by terrestrial organic material for LPM sediments. (**c**–**e**) Profiles demonstrating decrease in net-accumulation of low-Sr autochthonous $CaCO_3$ from the littoral to the profundal zone in LGM. (**f**) Estimate of the allochthonous

minerogenic sediment constituent (All_{inorg}) on $CaCO_3$-free base for an assumed Al_2O_3 content of 15.6 wt% of the bulk siliciclastic sediment fraction (Al_2O_3 value for mean continental crust composition after Taylor (*1964*), see (**g**) for Al concentration data). (**h**–**l**) Profiles of selected element ratios, characterizing the siliciclastic sediment fraction: La_N/Tm_N, ratio of Chondrite-normalized REE concentrations (used data for normalization from Taylor and McLennan (*1985*)). Distinctly enhanced Fe/Al, U/Al and Mo/Al values in the profiles from the 8 m sampling site reflect intense chemical alteration and re-distribution of Fe, U and Mo. Increase of Fe/Al and Mo/Al in the LPM sediments coinciding with S_{total} increase, (**n**) indicates sulphide-precipitation of Fe and Mo in the modern LPM, (**m**) excess Fe balanced for an assumed Fe/Al mass ratio of 0.9 for the minerogenic debris

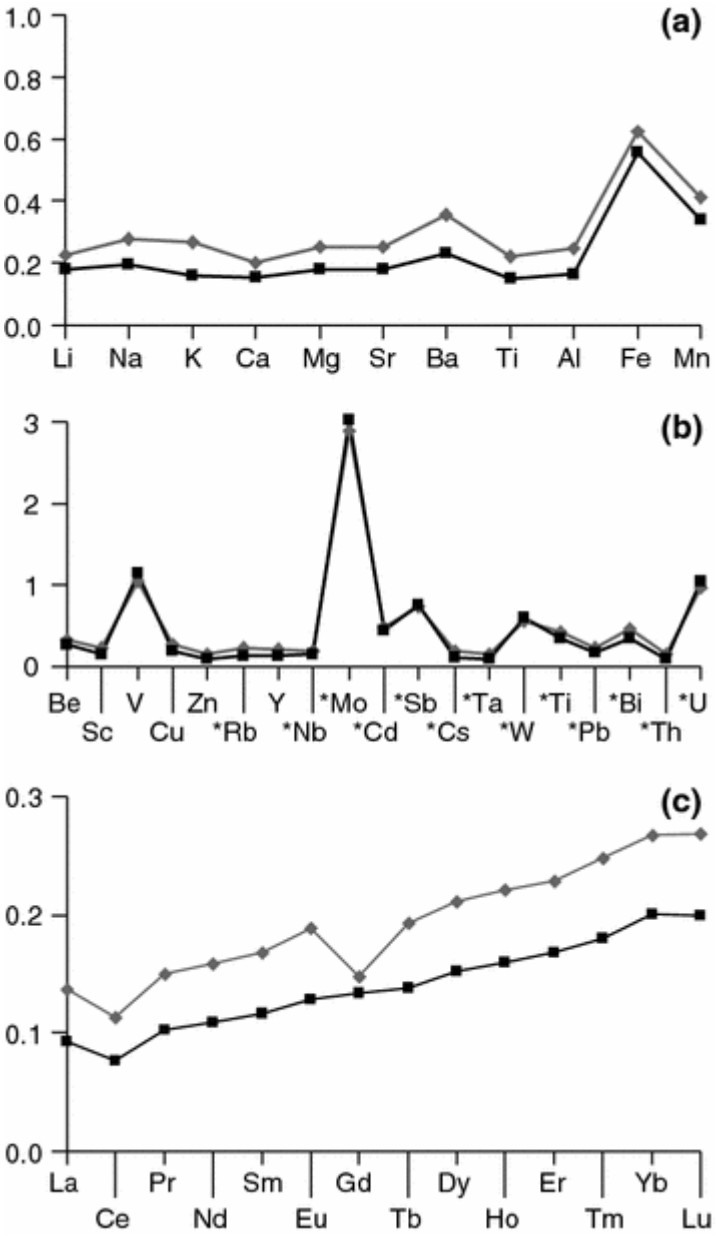

Fig. 6 (**a**–**c**) Concentration of selected major and minor elements in deeper sections of the 8 m core versus their average concentration values in the upper 10.5 cm sediment; minor depletion or enrichment is recorded for Fe and Mn and trace elements that form oxy-anions that can be scavenged by Fe-oxidhydroxides; depletion shows systematic increase from light to heavy REEs. Trace elements marked by * and REEs were measured by ICP-MS (Analyst: M. Zimmer, GFZ-Potsdam)

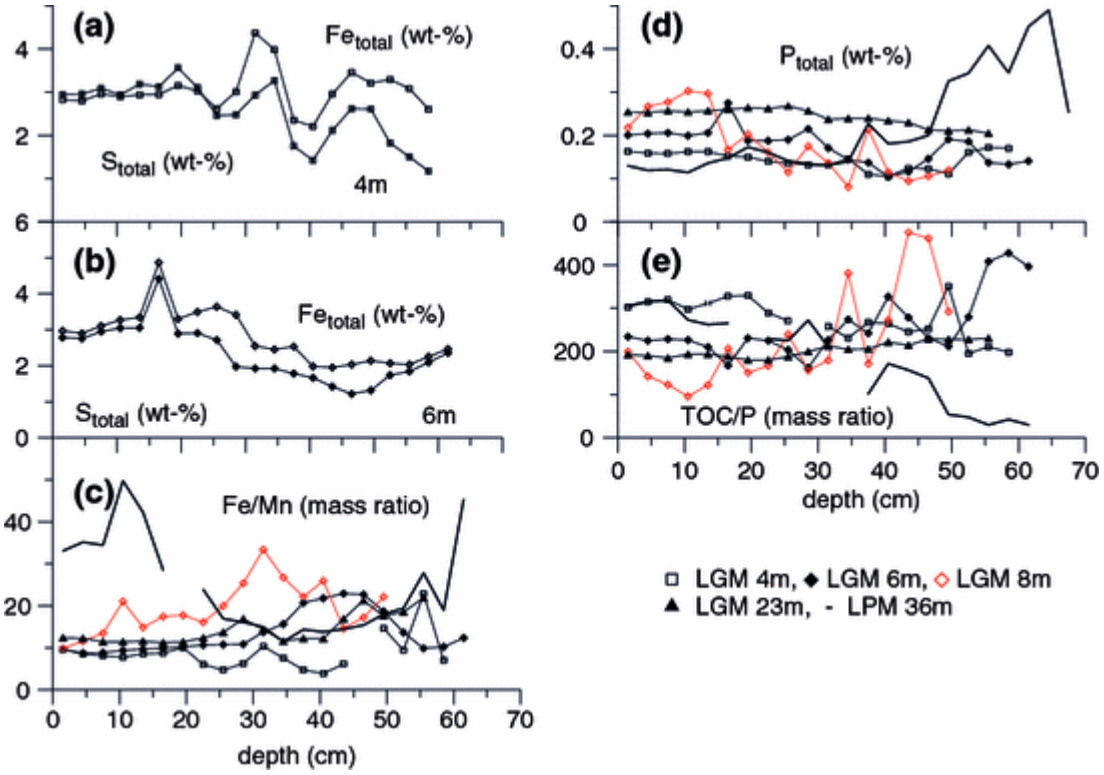

Fig. 7 Geochemical sediment profiles from the centre of LPM and from LGM cores. (**a**, **b**) Profiles, showing coincidence between Fe_{total} and S_{total} peaks in the sediment cores 4 m and 6 m from the shallow water area. (**c**) Fe/Mn fractionation in LPM and LGM. In the steeply inclining sector of the LGM basin, Fe is distinctly enriched versus Mn by precipitation of Fe-oxihydroxides. The dissolved Fe concentrations in the monimolimnion of LPM exceeded 100 mg/l in 1995 (Chiodini et al. *1997*); dissolved Fe is precipitated as FeS; formation of Fe(Mn,Ca)-carbonates is prevented by pH-lowering associated with high CO_2 concentrations in the deep water of the lake. (**d**, **e**) P_{total} and TOC/P profiles of LGM sediments document that the burial rate of P in the sediments from the lake centre is higher than that of littoral sediments

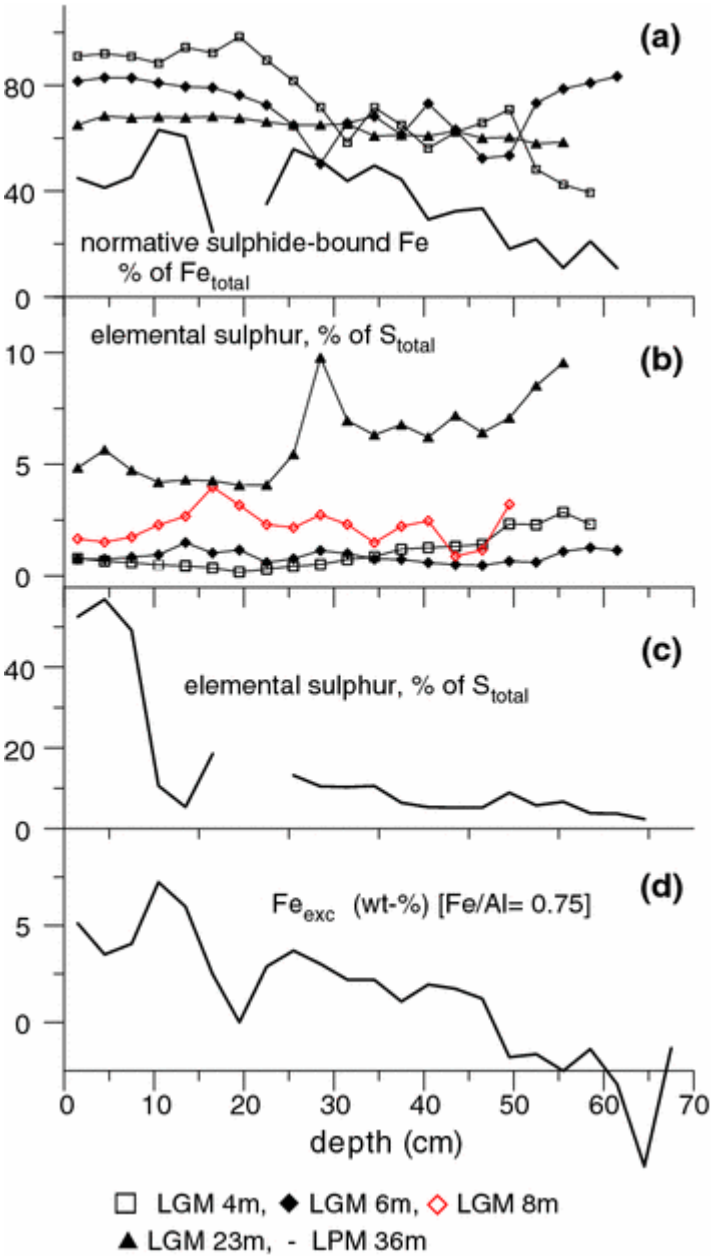

Fig. 8 Sulphur in LGM and LPM sediments. (**a**) Normative sulphide-bound Fe in percent of Fe_{total}; pyrite as the only sulphide phase and absence of organic-bound sulphur is considered for the estimate. (**b**, **c**) Analytical determined elemental sulphur in percent of S_{total} for LGM and LPM sediments. (**d**) Excess Fe in LPM sediments balanced for an assumed Fe/Al mass ratio of 0.75 for the siliciclastic debris. Littoral sediments of the modern LGM show slightly higher S_{total} contents than the sediments from the lake centre (Fig. 5n), documenting overall higher H_2S production in the shallow water area of LGM. Pore water dissolved H_2S is fixed in the sediments mainly by reaction with reactive Fe or oxidation to elemental sulphur. The above mass balance estimates show that the sedimentary Fe inventory is most claimed in shallow water sediments of LGM. Pyrite genesis in the shallow water sediments is favoured by distinct seasonal change between oxic and anoxic conditions in the surface sediments. In LGM sediments from the 23 m sampling site and in sediments of the meromictic LPM a high proportion of elemental sulphur was detected in the freeze-dried samples. The real elemental sulphur contents may be overestimated due to oxidation of S^{2-} to elemental sulphur during freeze-drying and sample handling

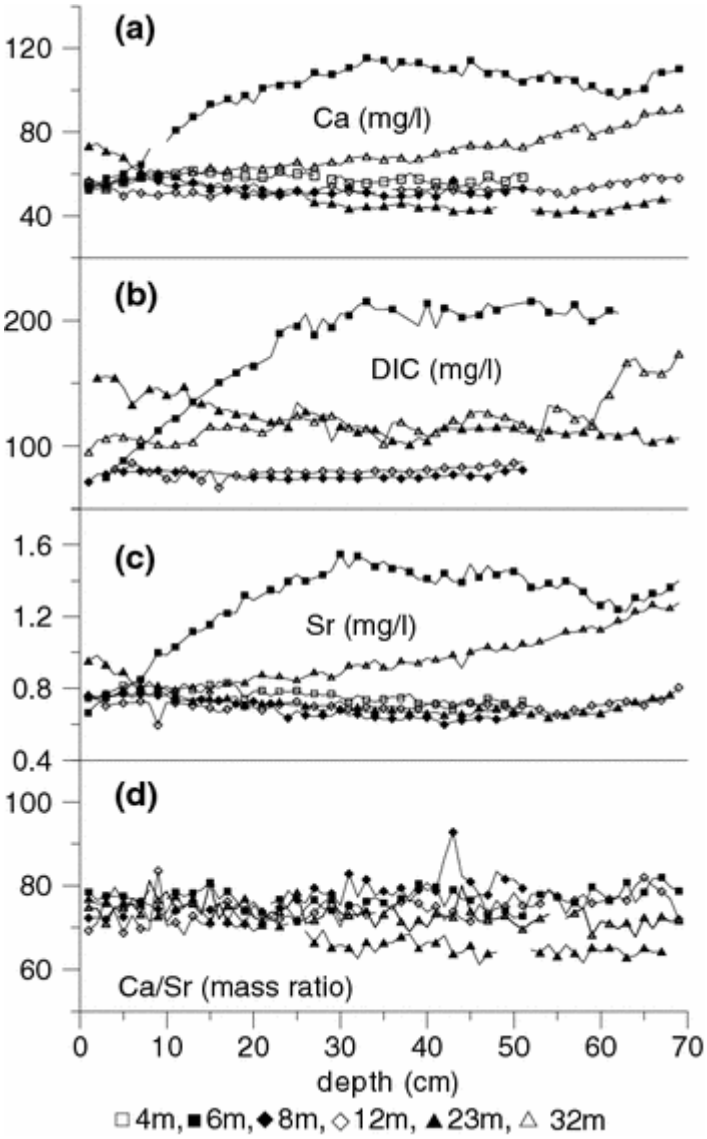

Fig. 9 (**a**–**d**) In situ pore water profiles of Ca, DIC, Sr, Ca/Sr of LGM sediments from various water depths at 1 cm resolution, sampling sites shown in Fig. 1b. Dialysis chambers were exposed between 23 August and 18 September 1994. Please note that each second data point is shown only for data presentation. Pore water profiles from the 12 m sampling site are exceptional. Relative enhanced post-depositional cation release from siliciclastic sediment components is mainly associated with differing diagenetic conditions in the steeply inclining sector of the LGM basin

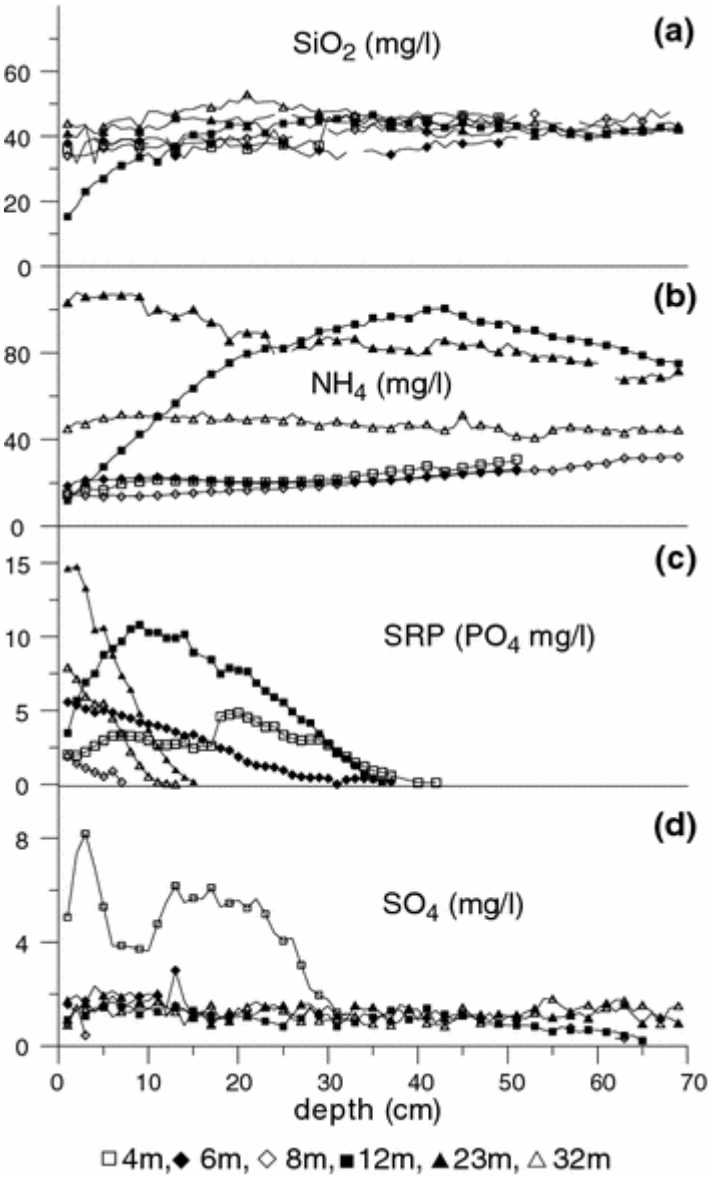

Fig. 10 (**a**–**d**) In situ pore water profiles of algae nutrients and SO_4 for LGM sediments from various water depths. Note that SO_4 pore water concentrations below 1.5 mg/l are not consumed, or possibly regenerated in the equilibrium with hauyne

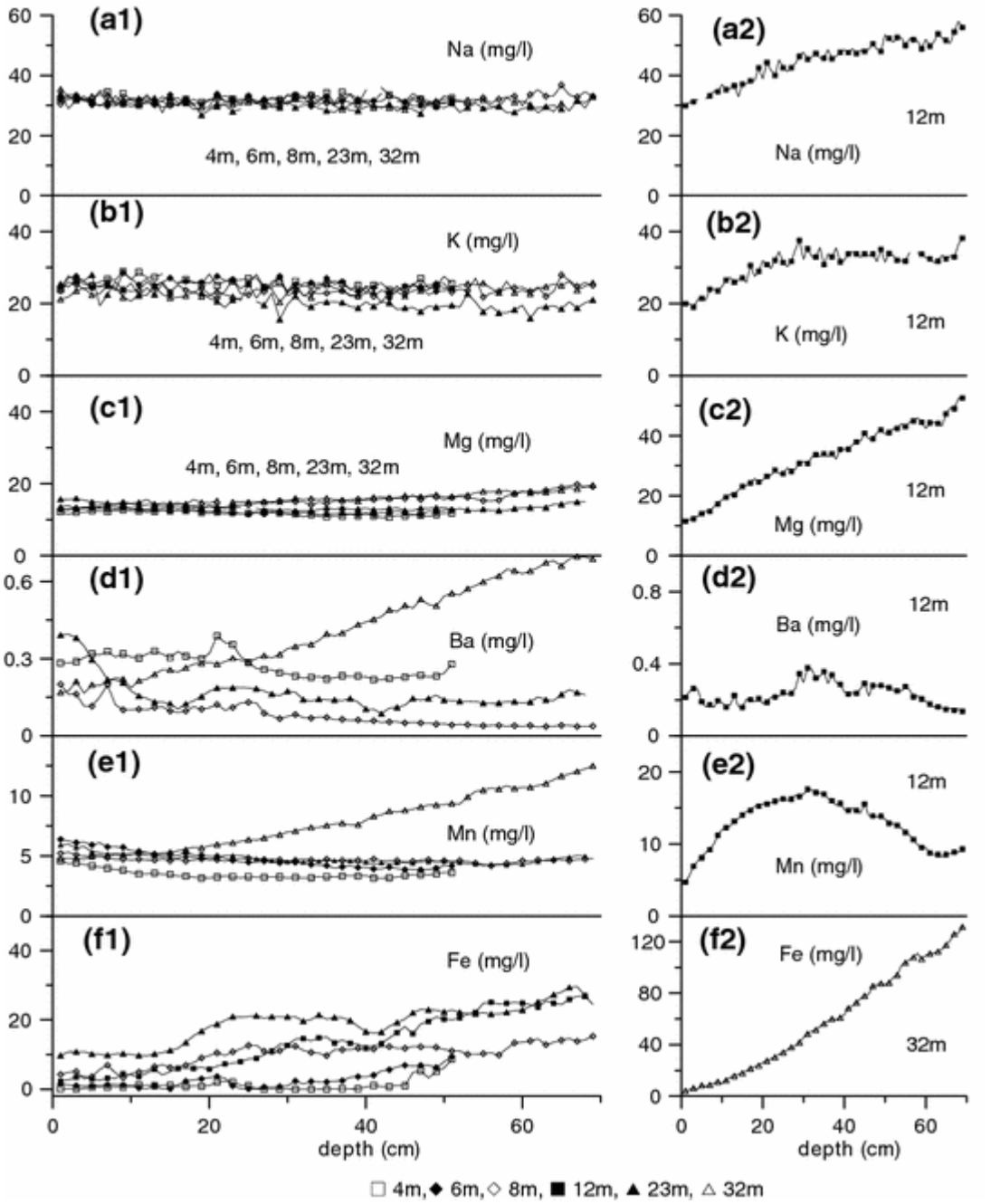

Fig. 11 (**a1/2**–**f1/2**) In situ pore water profiles of cations in LGM sediments from various water depths. Enhanced cation concentrations in the interstitial water of the steeply inclining sector of the LGM basin indicate high cation release by chemical alteration, which is also implied by the geochemical signatures of sediments from the 8 m site. The highest Fe concentrations are obtained in the pore water from 32 m; formation of authigenic Fe-minerals is inhibited by enhanced CO_2 contents and SO_4 depletion in the anoxic deep water of LGM

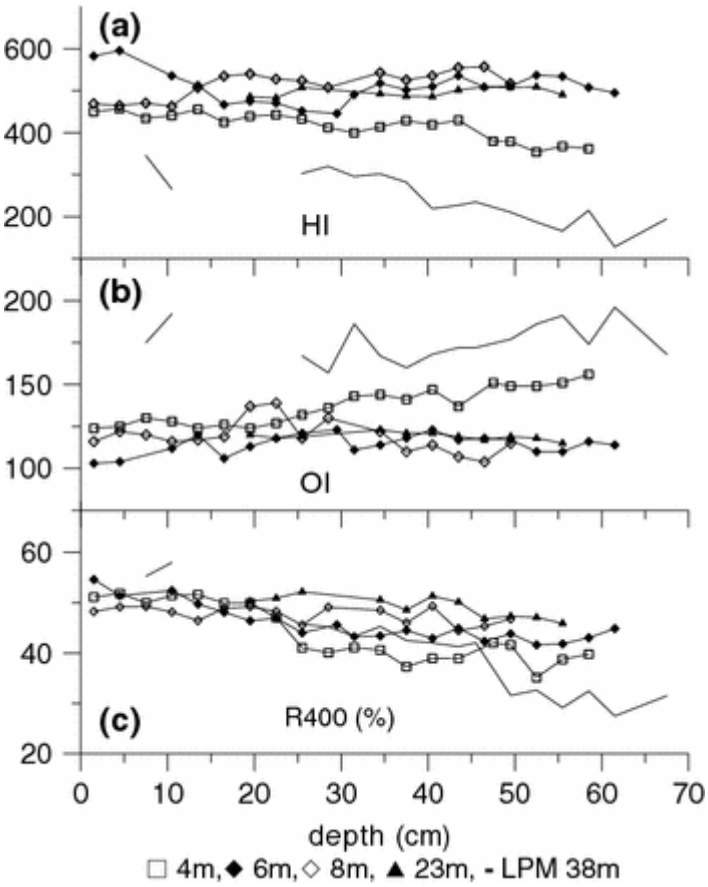

Fig. 12 (**a**–**c**) Results of RE analyses, HI—Hydrogen Index given in mg HC per g TOC, OI—Oxygen Index given in mg CO_2 per g TOC, R400—Pyrolysis products <400°C issued from Flame Ionisation Detection (FID) given as percentage of total pyrolysis products <650°C

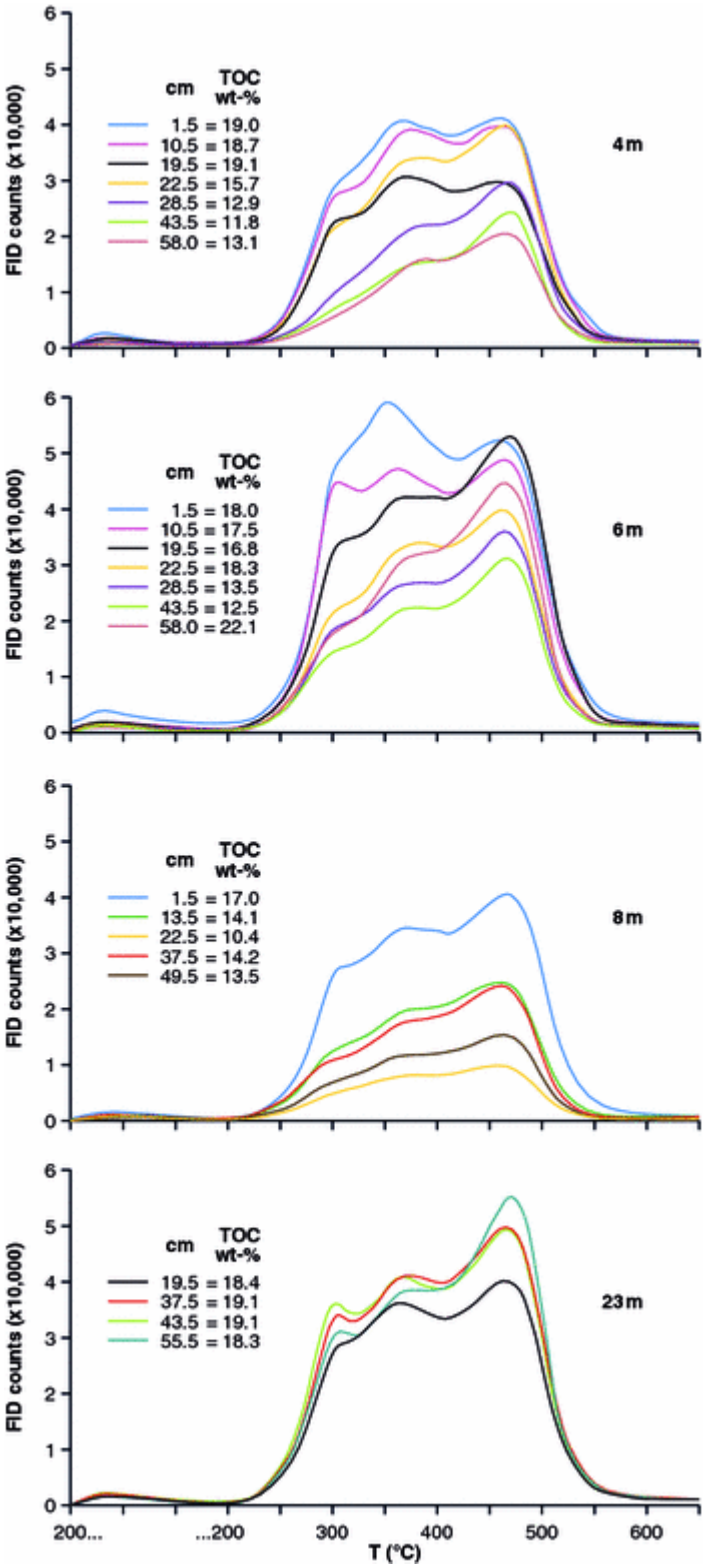

Fig. 13 FID heating curves of selected LGM sediments from various water depths, sediment depths and TOC contents of individual 3-cm samples are given inside the diagrams

Tables

Table 1 Unsupported ^{210}Pb data and derived ^{210}Pb ages

Depth (cm)	φ^a	$\rho_s{}^a$ (g/cm^3)	Model ages		Unsupported ^{210}Pb (mBq/g dry sed.)			
			CIC	CRS				
			LGM 4 m	LGM 6 m	LGM 4 m	LGM 6 m	LGM 23 m	LPM 36 m
1.5	0.990	2.0	1993		994	–	291	982
4.5	0.980	2.0			–	–	–	678
7.5	0.940	2.0	1987	1987	812	239	293	803
10.5	0.935	2.0			–	–	–	–
13.5	0.910	2.0	1976	1981	275	223	344	–
16.5	0.890	2.0			–	–	–	243
19.5	0.875	2.0	1958	1966	189	219	279	–
21.5	0.862	2.0		1963	–	–	–	–
25.5	0.852	2.0	1937	1953	133	167	242	
28.5	0.85	2.0			–	–	–	163
31.5	0.85	2.0	1915	1926	64	48	285	–
34.5	0.85	2.0			–	–	–	93
37.5	0.85	2.0		1908	38	30	321	–
40.5	0.85	2.0			–	–	–	58
43.5	0.85	2.0		1888	69	18	–	–
46.5	0.85	2.0			–	–	–	–
49.5	0.85	2.0		1859	56	–	249	–
52.5	0.85	2.0			–	21	–	58
55.5	0.85	2.0			65	–	313	–
58.5	0.85	2.0			–	−13	–	54

[a]Porosity and density of solid sediments considered for lead-210 dating, given activity data related to 1 September 1994

Table 2 Mineral composition silt LGM 6 m, siliciclastic fraction

Min. (%)/depth (cm)	Quartz	Augite	Leucite	Orthoclase	Plagioclase (Albite)
16.5	16	39	14	10	21
25.5	17	33	16	7	27
43.5	8	40	23	8	21
49.5	6	63	14	14	3
55.5	26	23	10	7	32